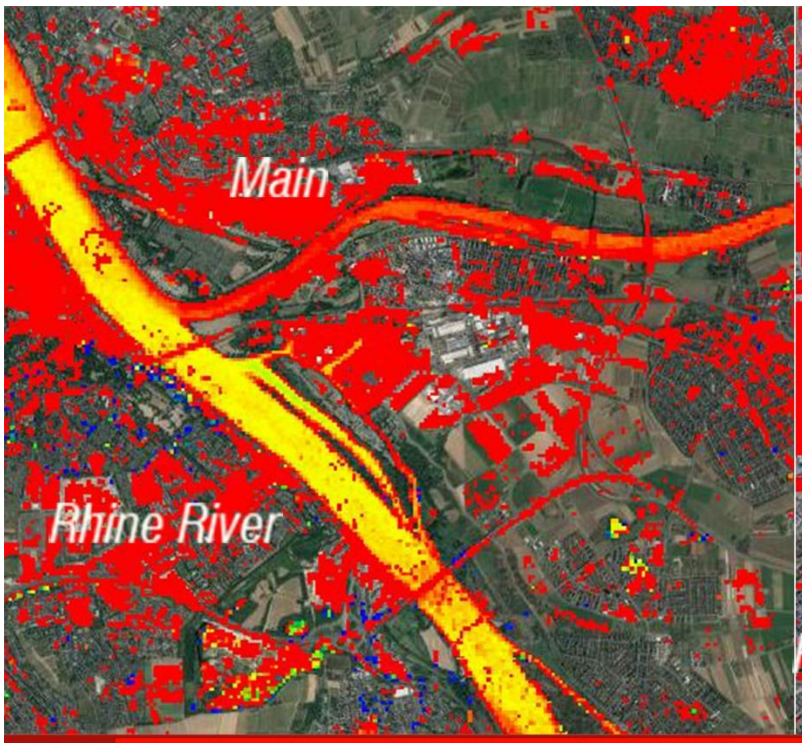

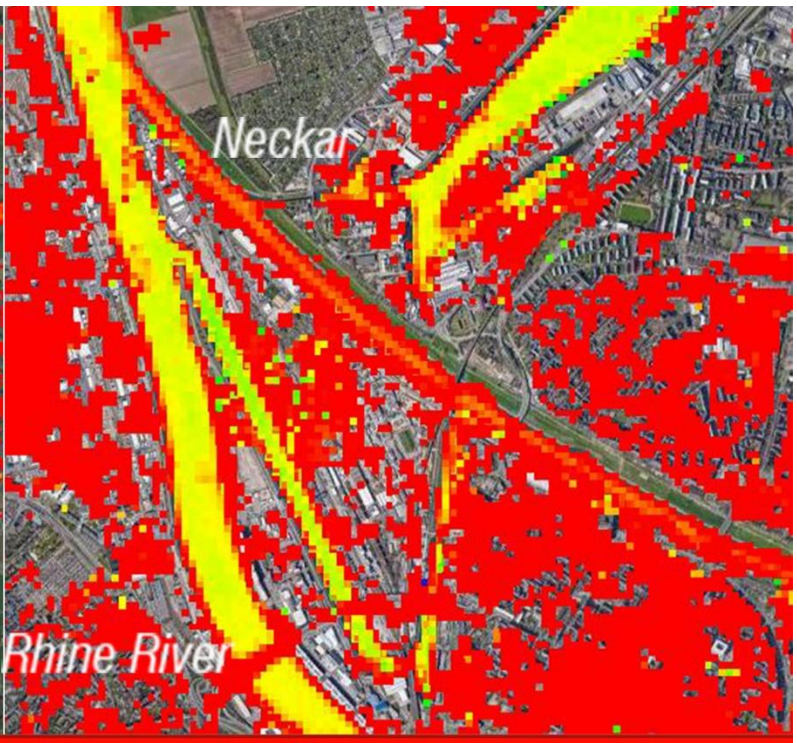

Msc Thesis

Monitoring of suspended sediment concentration in the Rhine River using Landsat (Google Earth Engine)

CUT AYU TIARA SUTARI

Utrecht University

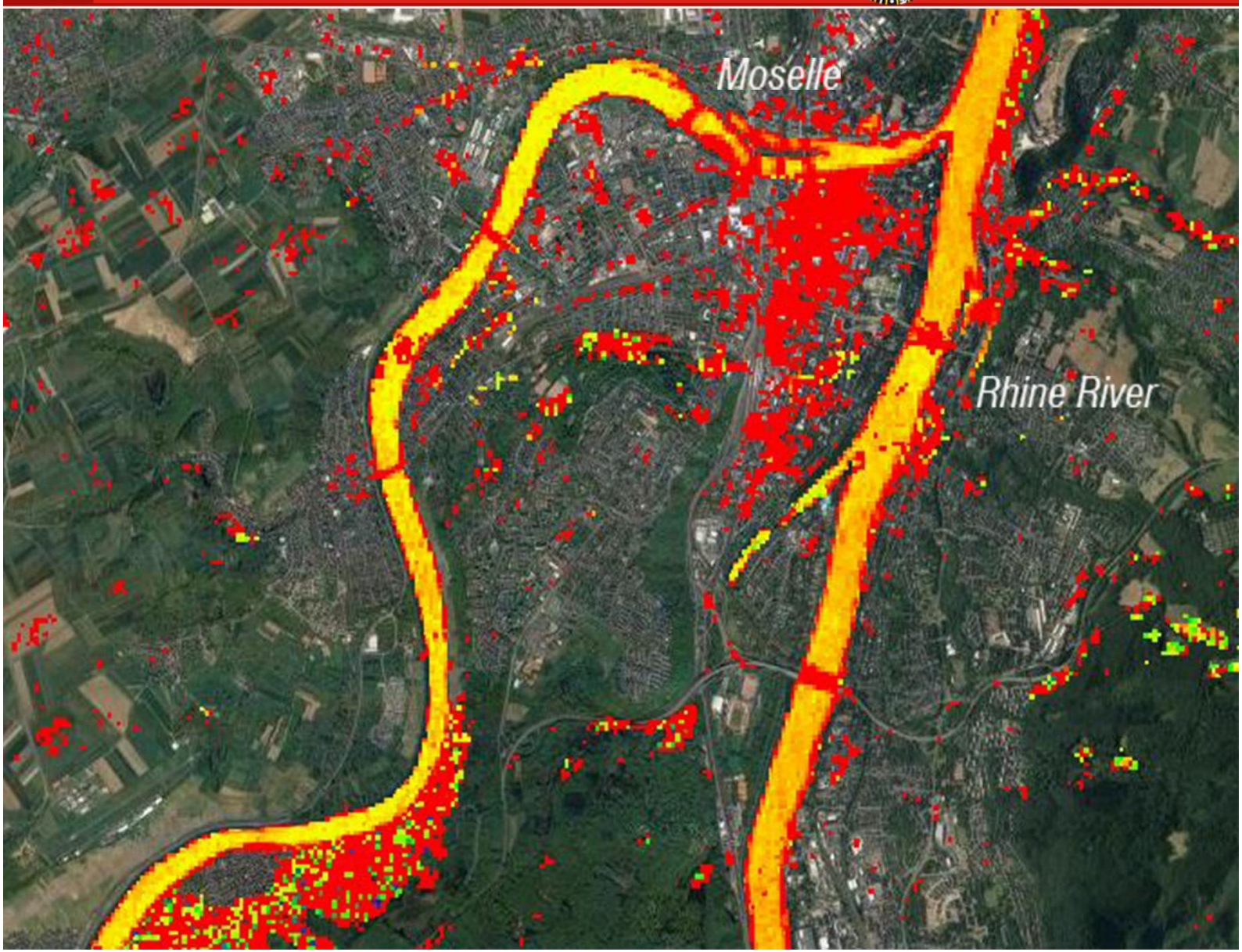

Monitoring of suspended sediment concentration in the Rhine River using Landsat (Google Earth Engine)

Cut Ayu Tiara Sutari

in fulfillment of the requirements for the degree of

Master of Science
Earth Surface and Water

Student number : 5858941

Supervisor :
Marcel van der Perk Utrecht University
Hans Middelkoop Utrecht University

Utrecht University

PREFACE

The completion of this MSc Research would not have been possible without the help and support of many people. First, I would like to thank my supervisor, Marcel van der Perk and Hans Middelkoop for all their help, advice, and support. Second, I would especially like to thank my husband Wachid and my baby Alby for their patience and support during the finalization of my thesis. I love you.

Cut Ayu Tiara Sutari,
Utrecht
April 2019

ABSTRACT

The traditional methods for measuring water quality are time-consuming and do not give a spatial and temporal view of SSC needed for assessment of the water quality. The prediction of the suspended sediment using remote sensing through the main channel and tributaries of Rhine River can provide valuable information to assess the sources of the suspended sediment under different hydrology condition. The main objective of this study is to understand the suspended sediment concentration (SSC) characteristics in the Rhine River using Landsat satellite images. This study developed a method of quantifying SSC based on Landsat imagery and corresponding SSC data from *Bundesanstalt für Gewässerkunde* (German Federal Institute of Hydrology) from 1995 to 2016. The model is built using the ratio of logarithmic transformation of a red/green band and logarithmic transformation of SSC based on *in-situ* sampling measurements. The SSC model works well and shows satisfactory performance. Landsat satellites (Thematic Mapper (TM), Multi-Spectral Scanner (MSS), Enhanced Thematic Mapper (ETM), Operational Land Imager (OLI)) explained an acceptable result accuracy (R^2: 0.32; error/ bias -0.02 mg/L; RMSE 12.23 mg/L; NSE 0.33). With the derived empirical regression, we produced Landsat-derived SSC maps for the 1995-2016 period. Analyses of images product suggest that the change of SSC shows a marked increase of about 6 mg/L at Upper Rhine, gradually increase of about 3 mg/L at Middle Rhine, and relative constant at Lower Rhine. Turning to seasonal variation, high SSC is mostly found in winter and low SSC is in summer. However, another result shows that the SSC tend to be high in June at almost all monitoring stations where the discharge is minimum. The major sediment source at Lobith was mostly regulated by the River Moselle in high discharge condition, which shows a *clockwise* loop. The major source of SSC at Lobith was mostly regulated by the Neckar River and Main River in moderate discharge condition since it is affected by exhaustion of the SSC in the channel and the travel time of the sediment supply from the tributaries. Another result in moderate discharge condition, *counter-clockwise* loop, indicates that the major sources of SSC were mainly from the Neckar River and Main River in moderate discharge condition. No hysteresis loop at low discharges shows the upstream tributaries input such as the Neckar River, the Main River, and the Moselle River contributed to almost equal amounts of SSC to the downstream. This type of hysteresis occurred relatively often during summer and SSC peak simultaneously, which suggest that Q–SSC relations are more controlled by the entrainment of bed material. The shape of the hysteresis loops is not only affected by exhaustion of the SSC in the channel, but also the travel time of sediment supply from the tributaries. The travel time for high discharge is one day, while for moderate and low discharge conditions is within 2-3 days.

Keywords: suspended sediment concentration, remote sensing, Landsat, google earth engine, Rhine River, suspended sediment, hysteresis

TABLE OF CONTENTS

LIST OF FIGURES

LIST OF TABLES

1. INTRODUCTION

Suspended sediment consists of organic and inorganic materials carried within the water column (Fryirs & Brierley, 2013). Suspended sediment is a natural and crucial component and plays a crucial role in the hydrological, ecological and geomorphological functioning of the river system (Guan et al., 2018). Suspended sediment can be a useful indicator for assessing the effect of land use changes and engineering practices in watercourses (Bisantino et al., 2011). Accelerated soil and bedrock erosion on hillslopes commonly results in elevated suspended sediment concentrations and loads in rivers (Woodward & Foster, 1997). The off-site problems can trigger local flooding, silting of local tile drains and damage to local properties, to a broad-scale problem in the catchment where the water column capacity reservoirs are threatened by the increased the sedimentation (Meade, 1982; Kothyari, 1996; Lahlou, 1988). In contrast, sediment deficit in rivers can also disrupt the continuum of sediment transportation process from river headwaters to deposition zone, which may produce severe alteration of river morphology, hydrology, ecology and damaging infrastructure (Batalla, 2003). The monitoring of suspended sediment in river is essential to provide information on sediment delivery and sustainable water management

Time series of suspended sediment were carried out at several main Rhine River sections and its tributary rivers for the period between 1995 and 2016. This *in-situ* measurement can give long record data availability. However, although such measurements are accurate in time and space, they do not give a detailed spatial and temporal view of SSC needed for assessment of the water (Ritchie et al., 2003). The prediction of the suspended sediment using remote sensing through the main channel and tributaries of Rhine River can provide valuable information to assess the sources of the suspended sediment under different hydrology condition. However, there are some limitations and uncertainties which would further describe in this study.

Recently, the remote sensing method can be used as an alternative method to predict the suspended sediment. Several techniques have been used to estimate the SSC from different remote sensing system. The method used to connect between *in-situ* measurements to the satellite observation with the statistical relationship have been used extensively to provide a robust estimate of SSC (Markert et al., 2018). The evidential relationship between the suspended sediments and radiance or reflectance from spectral wave band or the combination of wave bands on satellite and aircraft sensors have been demonstrated (Ritchie et al., 2003). Furthermore, several studies have found that first four bands of Landsat and the use of single band (Zheng et al., 2015) and band ratio (Markert et al., 2018) is well correlated with suspended sediments. Landsat sensors: Thematic Mapper (TM), Multi-Spectral Scanner (MSS), Enhanced Thematic Mapper (ETM), and Operational Land Imager (OLI) have been used fairly successfully to measure most of the important water quality parameters, such as suspended sediment (Gholizadeh et al., 2016).

Previous studies, Zheng et al. (2015), produced a significant positive correlation between *in-situ* measurements of suspended sediment and near-infrared band on Landsat OLI resulted in R^2=0.81 for Dongting Lake, China. Markert et al., (2018) tested several single bands and band ratio of Landsat satellite to estimate the suspended sediment in the Lower Mekong, producing variety R^2 from 0.305 to 0.505 from different model statistic. While these studies provide a

variety of correlation results, choosing empirical model built by bands satellite sensor and the used statistic methods needs careful consideration before a broad use.

Google Earth Engine offers an opportunity to use the real-time satellite to access the suspended sediment data without high-cost software installed. For the example, atmospherically corrected and georeferenced Landsat data are now accessible for free, and can be easily mosaicked, masked for clouds, and composited within Google Earth Engine platform (Google Earth Engine Team, 2015). Remote sensing data from Landsat satellite is used over 20-years period (1995-2016).

This study aims to understand the suspended sediment concentration (SSC) characteristics in the Rhine River using Landsat satellite images. Below are the research questions answered at the end of the report.

(1) How accurate does Landsat data predict the SSC in Rhine River?

(2) What are the spatial and seasonal variabilities of SSC from upstream to downstream Rhine River?

(3) What are the sources of suspended sediment in the Rhine River under high, moderate, and low discharge conditions?

The SSC model was built in several steps: first, data from SSC *in-situ* measurements were compiled from 1995-2016. Second, the reflectance value from Landsat satellite images was extracted to create the empirical model for predicting the SSC. Third, Landsat satellite images were correlated with SSC *in-situ* measurements which coincide on the same day producing matrix correlation. The highest correlations were attempted further to build the linear regression. Once the model was built, the model performance was evaluated using the coefficient of determination (R^2), error bias, Root Mean Square Error (RMSE), and Nash-Sutcliffe Efficiency (NSE). Data processing of SSC prediction was adopted from Markert et al., (2018). To understand the change of SSC, the river channel is divided into several sample locations, which lie 35 km per sections resulting in the longitudinal graph of SSC from upstream to downstream. The mechanism underlying suspended sediment transport during different hydrological conditions were characterized by hysteresis patterns to understand the different sources of supply in different parts of the study area. Furthermore, the earlier and later events of the discharge and SSC (hydrograph and sediment graph) were analyzed to shows further evidence for the change in the character of sediment transport.

2. METHODS

2.1 Study Area

The Rhine River is the second largest river in Europe and has a total catchment area of 165.000 km^2. The river originates from European Alps with the total length of the river 1320 km to the North Sea and its annual discharge near the mouth is 2500 m^3/s. The largest discharge is at the Lower Rhine with a maximum discharge approximately 12.000 m^3/s and the minimum discharge with only 267 m^3/s at the Upper Rhine. In summer, water mostly comes from snowmelt in the southern part of the drainage basin. In winter, the central part of the Rhine River gives a substantial water contribution to downstream.

Fig.2.1 and Fig.2.2 show longitudinal profile and geological-hydrological longitudinal section of the Rhine River which affect the specific condition for the riverbed gradient. At the top of Rhine, the river starts at Lake Constance which is flat (0.8 ‰). The slope decreases consistently from upstream to downstream and becomes nearly zero to the North Sea.

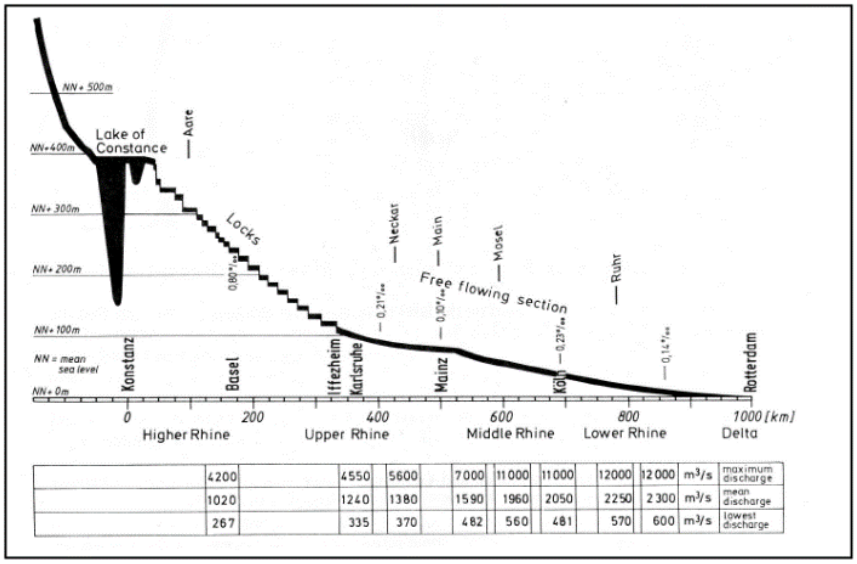

Fig. 2.1. Longitudinal profile of the Rhine and location of floodplains after CHR 1987 (Spreafico & Lehmann, 2009)

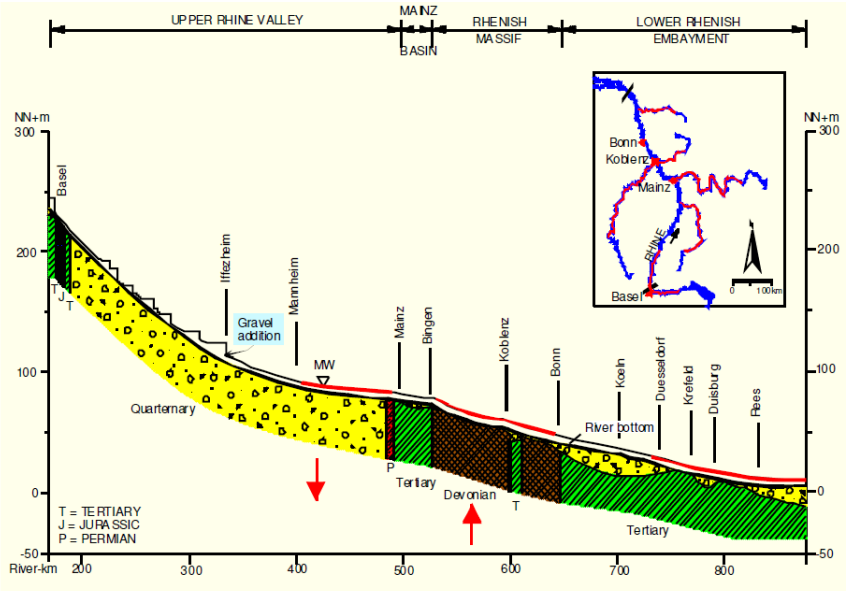

Fig. 2.2. Geological – hydrological longitudinal section, Basel – Emmerich (Spreafico & Lehmann, 2009)

The most upstream of the Rhine river, consisting of the Alpine Rhine and High Rhine, is predominantly composed of Mesozoic sedimentary rock. Reaching to Basel, the landscape surrounding the river changes drastically. The condition from Basel to Mainz is characterized by Paleozoic sediment. The Rhine then enters the Upper Rhine Graben, which shifted from the Mesozoic granite in the Graben to limestone geological units (Preusser, 2008). When the Rhine leaves the Rhenish Massif, the downstream part of the catchment begins, consisting of Lower Rhine and Rhine Delta. Tertiary and Quaternary sediments are well in the Lower Rhine.

The Rhine River has been increasingly affected due to human impact over many centuries. About 50 million people live in the Rhine River basin, of which 60% live in Germany and 20% in the Netherlands. Moreover, transportation and engineering works have been intensively practiced since in the Middle Ages. Intervention on the landscape, such as deforestation, population growth, and climate change have been increasing significantly. People built engineering works such as weirs and water mills (Bormann et al., 2011) and dike to protect flood (Buck et al., 1993). In the century afterward, the river was embanked entirely (Schmidt, 2000). Weir construction resulted in bed degradation and some parts of the Rhine River were channelized and protected in the 19th century (Wenka, 2009). Moreover, the river had been narrowed and straightened to increase the accessibility of the shipping route (Frings et al., 2014). In the 20th centuries. Small engineering works such as flood protection construction and dams built in several tributaries river were built to generate power (Uehlinger et al., 2009). A recent study on sediment fluxes in Rhine River has revealed that sediment has been dredged and re-allocated to from km 325 to km 625 and coarse materials have been supplied to stabilize the riverbed and to stop the bed degradation (Frings et al., 2014).

2.2 SSC Measurements

Suspended Sediment Concentration (SSC)

Bi-weekly SSCs are available at several main Rhine River monitoring stations: Weil am Rhein, Lauterbourg, Koblenz Rhein, and Bimmen, which have been registered by the International Commission for the Protection of the Rhine (IKSR). For Lobith, daily SSC was provided by the Dutch Rijkswaterstaat from 1995 to 2016. Table 2.1 shows the records for IKSR monitoring stations. Fig.2.3 shows the locations where *in-situ* SSC observation data, discharge data, and SSC model are provided. The SSC from measurements are used to create and evaluate the SSC model using spectral data from satellite imagery.

Table 2.1. IKSR monitoring stations on the Rhine River

Station	River km	Location
Rekingen	90.7	Swiss monitoring station above the Aare River confluence
Weil Am Rhein	174	Swiss station beneath Basel
Lauterbourg	359	French station above German/French border
Koblenz Rhein	590.3	German station above Mosel confluence
Lobith	863	Dutch station at a border to Germany
Bimmen	865	German station at a border to the Netherlands

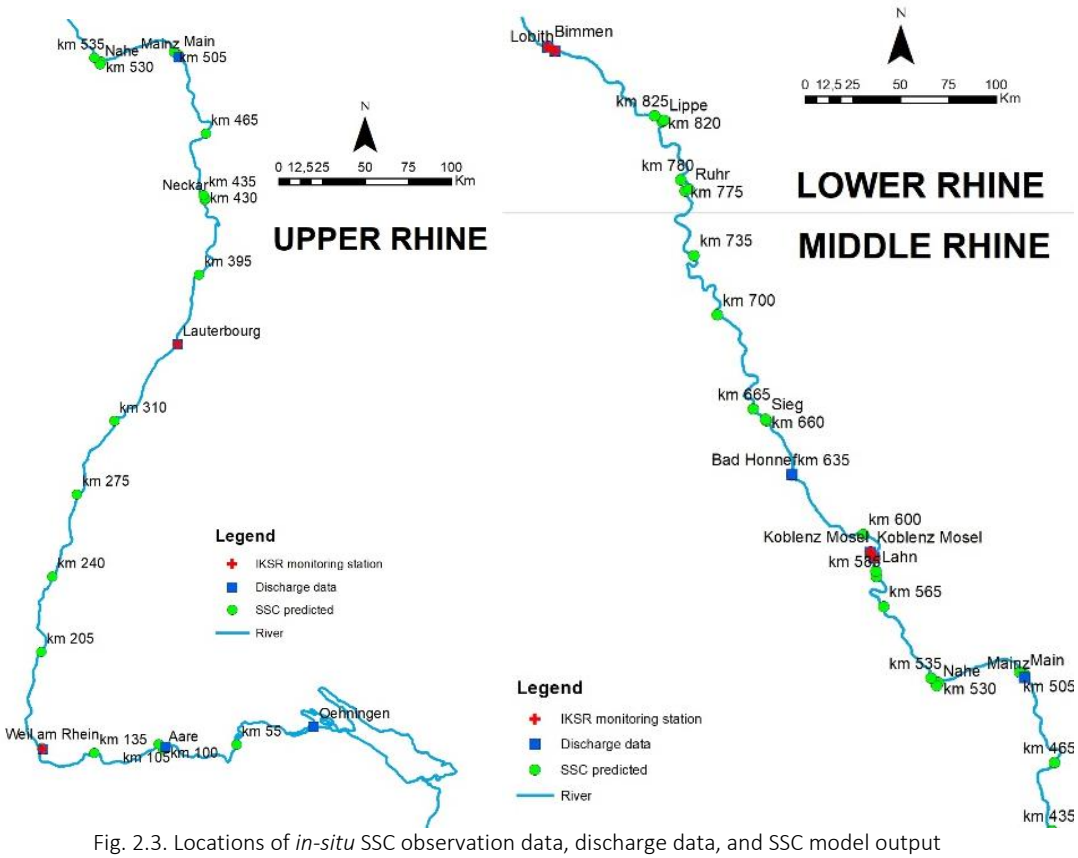

Fig. 2.3. Locations of *in-situ* SSC observation data, discharge data, and SSC model output

Landsat Imagery

Landsat satellite was chosen for this study due to wide range spatial and temporal data availability for Rhine River and has acceptable spatial resolution 30-meter x 30-meter to mapping large rivers. Four Landsat sensors were used in this study, Landsat 4 and Landsat 5 Thematic Mapper (TM), Landsat 7 Enhanced Thematic Mapper Plus (ETM+), and Landsat 8 Operational Land Imager (OLI). All Landsat satellites move from north to south over the sunlit side of the Earth in synchronous orbit. Each satellite crosses every point on Earth once every 16 days with 8 days offset data acquisition, while two Landsat satellites were in operation. The Landsat satellite was chosen for this study ranging from 1995 to 2016.

2.3 Data Pre-processing and Data Masking

The method for SSC prediction was carried out in the following steps (Fig.2.4). First, data from SSC *in-situ* measurements were compiled from 1995-2016. Second, the reflectance value from Landsat satellite images was extracted to create the empirical model for predicting the SSC. Third, Landsat satellite images were correlated with SSC *in-situ* measurements which coincide on the same day producing matrix correlation. The highest correlations were attempted further to build the linear regression. Once the model was built, the model performance was evaluated using the coefficient of determination (R^2), error bias, Root Mean Square Error (RMSE), and Nash-Sutcliffe Efficiency (NSE). Data processing of SSC prediction was adopted from Markert et al., (2018).

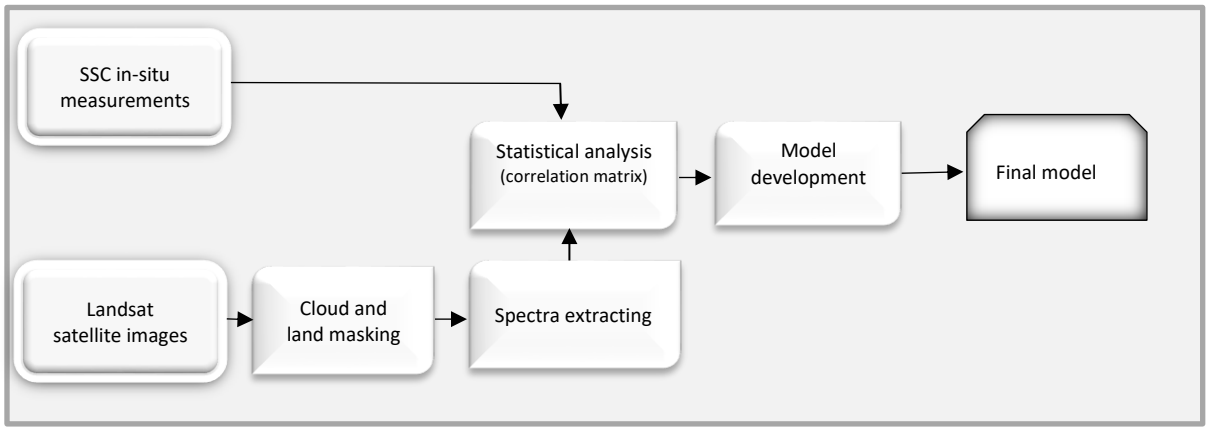

Fig. 2.4. Flowchart of the methodology

Water levels in the Rhine River are not always the same. To reduce the influence of channel bottom or upwelling that occurs next to the river bank and in shallow water, sampling locations were filtered to ensure that only SSC of at least 60 m (two Landsat pixels) from the bank of the water body was involved in further analysis. To account for the river morphology changes from 1995-2016, the shoreline was dynamically measured from the European Commission's Joint Research Center (JRC) MonthlyWater History v1.0 image collection (JRC/GSW1_0/MonthlyHistory) (Pekel et al., 2016). SSC sample locations collected within 60 m of the dynamic shoreline were not applied in the analysis.

Data from the Landsat TM (from both Landsat 4 and 5 satellites), ETM+ (Landsat 7) and OLI (Landsat 8) sensors in this study have been corrected using Earth Resources Observation and Science (EROS) Center Science Processing Architecture (ESPA) surface reflectance which use the most mature approach Landsat Ecosystem Disturbance Adaptive Processing System (LEDAPS). LEDAPS accounts for scene spectral variations caused by atmospheric effects including ozone concentration, column water vapor, elevation and surface pressure, and aerosol optical thickness was processed by LEDAPS to convert digital numbers to top-of-atmosphere reflectance and apply an atmospheric correction using the 6S method resulting the surface reflectance (Masek et al., 2006). The surface reflectance is a complicated and robust correction that account for per pixel adjustment to create consistent radiometric response between and within images (Hansen & Loveland, 2012; Vermote et al., 2002). By removing the atmospheric effects, this allows the all scene to be treated based on application standard models (Vermote et al., 1997).

CFmask algorithm allows us to filter poor quality observations of each Landsat imagery (Chen et al., 2017). CF mask algorithm designates for each pixel of an image whether it is "clear" or affected by the occurrence of clouds, cloud shadows, snow or water (Zhu et al., 2015). In this study, CFmask pixel QA band acts to mask the cloud and cloud shadow in the Landsat images. Only 100% cloud-free of each Landsat scene was used in model development to avoid the effects of cloud cover as clouds represent highly unreliable values. Moreover, CFmask QA band was applied to extract pixels flagged as water as a secondary backup algorithm for Landsat scenes to fill the gaps between the JRC data availability

(JRC/GSW1_0/MonthlyHistory). The JRC water mask was applied to extract water only pixels for the analysis. However, since this study used time analysis from 1995 to 2016, the JRC data only exist from 16 March 1984 to 18 October 2015 which indicates that time analysis is out of JRC range availability.

Once the satellite images and in-situ measurements were checked and the satellite images were masked, the spectral bands from the Landsat were extracted from the corresponding Landsat scene. Finally, the logarithmic transform between image spectra band and *in-situ* measurements were then used to predict the SSC.

2.4 Data Processing

2.4.1 Statistical Methods

Multiple spectral bands and their ratios are extensively used to quantify water quality product (Gholizadeh et al., 2016). The spectral band ratios reduce the atmospheric, irradiance, and air-water surface influences in the remotely sensed signal (Lillesand et al., 2014). The spectral data from possible bands and band ratio were correlated to the SSC datasets to detect acceptable band or acceptable band ratio for SSC model. The correlation matrix was calculated using particular band or band ratio and suspended sediment. This correlation matrix table has been known as a powerful tool to summarize a large dataset and to identify and visualize pattern in the given data. The bands or band ratios with the highest correlation with the *in-situ* measurements are then evaluated further for estimating the SSC.

2.4.2 Model Development

To determine the best band or band ratio of SSC model, a correlation between SSC *in-situ* measurements and spectra from all possible bands and band ratios were correlate using table correlation matrix (Table 3.1). In this study, the highest correlation then was aimed to establish the regression model using ordinary least squares regression method. Several SSC regression models have been proposed in several previous studies (Markert et al., 2018; Pham et al., 2018; Qiu et al., 2017; Yepez et al., 2018). However, a customized regression model is needed to estimate the SSC in Rhine River, since there are many characteristic variations in particle size, density, and optical complexities of each water body (Bowers et al., 2009).

The average relation between band/band ratio and SSC is the form of exponential relationship (*equation* 2.1). The ordinary least squares regression method was used to make a regression of *a* and *b* coefficient. However, the underestimates come when the suspended sediment concentration is predicted using band or band ratio. Therefore, the bias correction (*CF*) is then used to correct underestimation (*equation* 2.2). However, a correction factor is mainly concern errors in the a-coefficient (Fergusson, 1986). The estimated $SSC^{correct}$ (equation 2.3) then is calculated by multiplying 10^a and SSC (*equation* 2.1) by CF (equation 2.2).

$$SSC = a\,X^{b} \quad (2.1)$$

$$CF = exp\,(2{,}651 * S^2) \quad (2.2)$$

$$SSC^{correct} = 10^{a} * SCC * CF \quad (2.3)$$

Where S^2 is the mean square error of the log-transformed regression (in log-10 units) and X is band or band ratio.

The result is evaluated by calculating the coefficient of determination (R^2), error bias, Root Mean Square Error (RMSE), and Nash-Sutcliffe Efficiency (NSE). R^2 describes the proportion of the variance in measured data explained by the predicted data. The error bias is the difference

between the predicted SSC value and the observed (*in-situ* SSC measurements). RMSE indicates error in the units (or squared units) of the model. The Nash-Sutcliffe Efficiency (NSE) is a normalized statistic that determines the relative magnitude of the residual variance ("noise") compared to the measured data variance ("information") (Nash & Sutcliffe, 1970). The SSC data for creating and evaluating the model used the same range of 1.5 mg/L to 120 mg/L.

2.5 Data analysis

To understand the change of SSC, the river channel is divided into several sample locations, which lie 35 km per sections. For tributaries, the sample locations of SSC are chosen at several meters before the confluence with the main channel of the Rhine River. in total, there are 35 sample locations at the main channel and 6 samplings are for the tributaries (the Neckar River, the Main River, the Nahe River, the Moselle River, the Sieg River, and the Ruhr River). To get SSC value for each sampling site, the average reflectance value of pixels surrounded are calculated (Fig.2.5).

Fig. 2.5. Average of reflectance values are calculated to derive SSC

In the result analysis section, the Rhine River then is divided into three major reaches. The first reach is the Upper Rhine, which covers from 0 kilometers until Mainz. The major tributaries in the upper reaches are Aare and Neckar. The second is the Middle Rhine, which extends from km 500 (Mainz) to km 735. There are two major tributaries join in the middle reaches. Main and Moselle play an essential role in regulating the Rhine sediment discharge. The final major reach is the Lower Rhine, which lies between km 735, and Bimmen, which owns several small tributaries, which are Ruhr and Lippe.

3. RESULTS

3.1 SSC Retrieval Model

All possible bands and band ratios that have the highest correlation coefficient of 0.53 are $\frac{red:green}{2}$, $\frac{red}{blue}$, and $\frac{red}{green}$. Several studies have suggested to use $\frac{red}{green}$ band to model SSC in surface waters (Markert et al., 2018; Pham et al., 2018; Qiu et al., 2017). Therefore, $\frac{red}{green}$ was chosen in this study to build the empirical model.

Table 3.1. Correlation matrix for log-spectral values each band and log SSC

	SSC	blue	green	NIR	red	$\frac{blue}{green}$	$\frac{blue}{red}$	$\frac{blue}{NIR}$	$\frac{green}{red}$	$\frac{green}{NIR}$	$\frac{red}{NIR}$	$\frac{NIR}{green}$	$\frac{green+red}{2}$	$\frac{red/green}{2}$	$\frac{red}{blue}$	$\frac{red}{green}$
SSC	1.00															
blue	0.22	1.00														
green	0.39	0.88	1.00													
NIR	0.22	0.68	0.62	1.00												
red	0.49	0.84	0.96	0.61	1.00											
$\frac{blue}{green}$	-0.29	0.42	-0.06	0.25	-0.07	1.00										
$\frac{blue}{red}$	-0.53	0.05	-0.36	-0.04	-0.50	0.79	1.00									
$\frac{blue}{NIR}$	-0.12	-0.09	-0.10	-0.79	-0.13	0.01	0.09	1.00								
$\frac{green}{red}$	-0.53	-0.44	-0.51	-0.38	-0.74	0.06	0.65	0.15	1.00							
$\frac{green}{NIR}$	0.00	-0.24	-0.07	-0.83	-0.10	-0.37	-0.21	0.93	0.11	1.00						
$\frac{red}{NIR}$	0.16	-0.11	0.08	-0.71	0.12	-0.38	-0.40	0.87	-0.19	0.96	1.00					
$\frac{NIR}{green}$	0.00	0.24	0.07	0.83	0.10	0.37	0.21	-0.93	-0.11	-1.00	-0.96	1.00				
$\frac{green+red}{2}$	0.43	0.87	0.99	0.62	0.98	-0.06	-0.41	-0.11	-0.60	-0.08	0.10	0.08	1.00			
$\frac{red/green}{2}$	0.53	0.44	0.51	0.38	0.74	-0.06	-0.65	-0.15	-1.00	-0.11	0.19	0.11	0.60	1.00		
$\frac{red}{blue}$	0.53	-0.05	0.36	0.04	0.50	-0.79	-1.00	-0.09	-0.65	0.21	0.40	-0.21	0.41	0.65	1.00	
$\frac{red}{green}$	0.53	0.44	0.51	0.38	0.74	-0.06	-0.65	-0.15	-1.00	-0.11	0.19	0.11	0.60	1.00	0.65	1.00

The regression results in the following equation to estimate the suspended sediment:

$$SSC = 30.03X^{3.3187} \quad (3.1)$$

where X = $\frac{red}{green}$, the equation then was used to create the model (Fig. 3.1) and to evaluate the model. The bias correction is already used to correct underestimation for the equation 3.1. However, the linear fit produces a low coefficient correlation which is 0.3, The standard error is 0.28 mg/L that is considered as an acceptable value (Moriasi et al., 2007). Table. 3.2 shows the error statistics to create the empirical model.

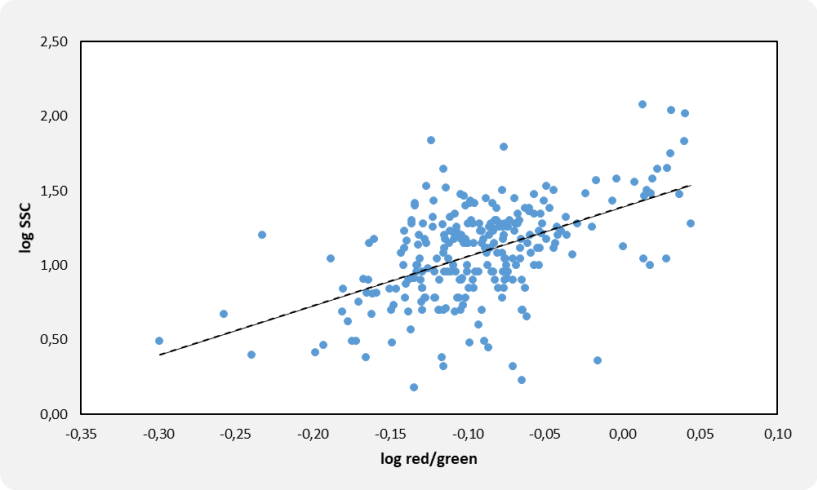

Fig. 3.1.Model calibration using the red/green band ratio with linear fit from Equation 1

Table 3.2. Error statistics of empirical model

R^2	intercept	gradient	st. error (mg/L)
0.30	1.39	3.32	0.28

3.2 Model Evaluation

SSC in the model evaluation ranged widely from 1.5 mg/L to 120 mg/L (Fig. 3.2). The SSC retrieval model results in a higher R^2, RMSE, and NSE values for 0.43, 11.08 mg/L, and 0.38 respectively in the wet season than in dry season 0.30, 12.66 mg/L, and 0.29 respectively (Table 3.3). However, the model produced in the dry season obtains higher error/ bias than in the wet season, which is 1.01 mg/L and -2.60 mg/L respectively. Meanwhile, error statistics for all validation dataset and wet season produce a coefficient of determination (R^2) lower than 0.5, which is considered unacceptable. However, error statistics model such as Nash-Sutcliffe model efficiency coefficient (NSE) and Root Mean Square Error (RMSE) of the entire datasets and season variations are well within an acceptable model range based on (Moriasi et al., 2007). The bias of the model is -0.02 mg/L for the entire datasets, indicating that the model performs well in estimating SSC for the overall average.

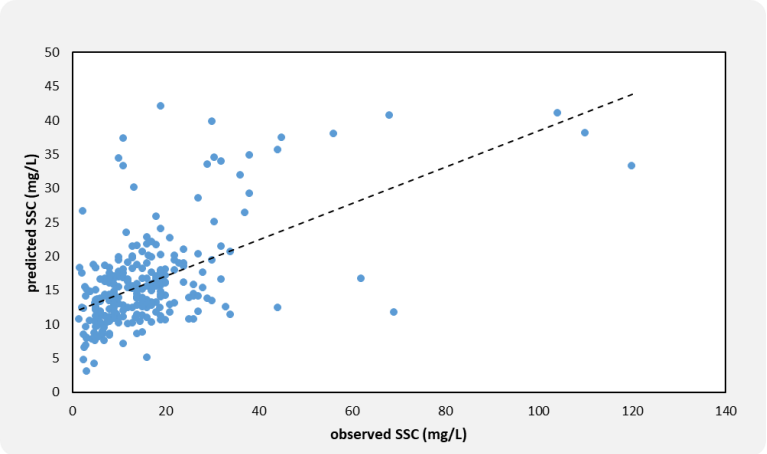

Fig. 3.2.Validation of empirical model compared to the validation dataset

Table 3.3. Error statistics for validation of empirical model compared to the validation dataset

	R^2	error/bias (mg/L)	RMSE (mg/L)	NSE (-)
wet	0.43	-2.60	11.08	0.38
dry	0.30	1.01	12.66	0.29
total	0.32	-0.02	12.23	0.33

3.3 Variation of Suspended Sediment Concentration 1995-2016

3.3.1 Spatial Pattern

a. Suspended Sediment Concentration

The changes in SSC are presented as daily averages (Fig. 3.3). In this study, the averages of SSC at Upper Rhine, Middle Rhine, and Lower Rhine are composed of 28 dates, 31 dates, and 32 dates, respectively. Furthermore, to know the dispersion of the data, SSC is also presented by five other statistical parameters, which are minimum, 25th perc., 50 th perc., and 75th perc. These statistics are calculated from the average SSC from all data.

The SSC shows a marked increase of about 6 mg/L at the Upper Rhine. There is a gradual increase of about 3 mg/L at Middle Rhine, and relative constant at the Lower Rhine on both selected dates and entire data. The averaged SSC on selected dates and entire data are 8.5 mg/L and 10.4 mg/L, respectively, at the Upper Rhine, 13.2 mg/L and 15,1 mg/L at the Middle Rhine and 14.9 mg/L and 16.8 mg/L at Lower Rhine. This pattern is also followed by other statistical parameters that is shown as representatively illustrating the data, except for the minimum. The minimum values of SSC show far out values in the distribution of SSC. This can be recognized as a high variation of SSC from 1995 to 2016.

SSC increased in the downstream direction, especially at tributary confluence locations. The first sudden jump is identified at Maxau and followed by the Neckar River at Upper reaches. There is a substantial 20% increase of SSC from Maxau (km 395) to km 430 based on both selected data and entire data calculations. Meanwhile, the Neckar River is found to be less contributing to the increase of SSC, with only 8% calculated from the entire data and 8% of decrease from the selected date. A small range of calculations may cause the anomaly of decrease from the selected dataset. At Middle Rhine, the Main River delivers substantial SSC of approximately 1 mg/L for both entire and selected datasets. Meanwhile, the transport of SSC from Moselle increased strongly to about 10% for both datasets. Further downstream, the changes of SSC are much stable and disappeared completely after km 735, without sudden any jump at tributary confluences, where several small tributaries such as the Ruhr River, the Lippe River, and the Sieg River lie at the Rhine River.

Upper Rhine	Middle Rhine	Lower Rhine

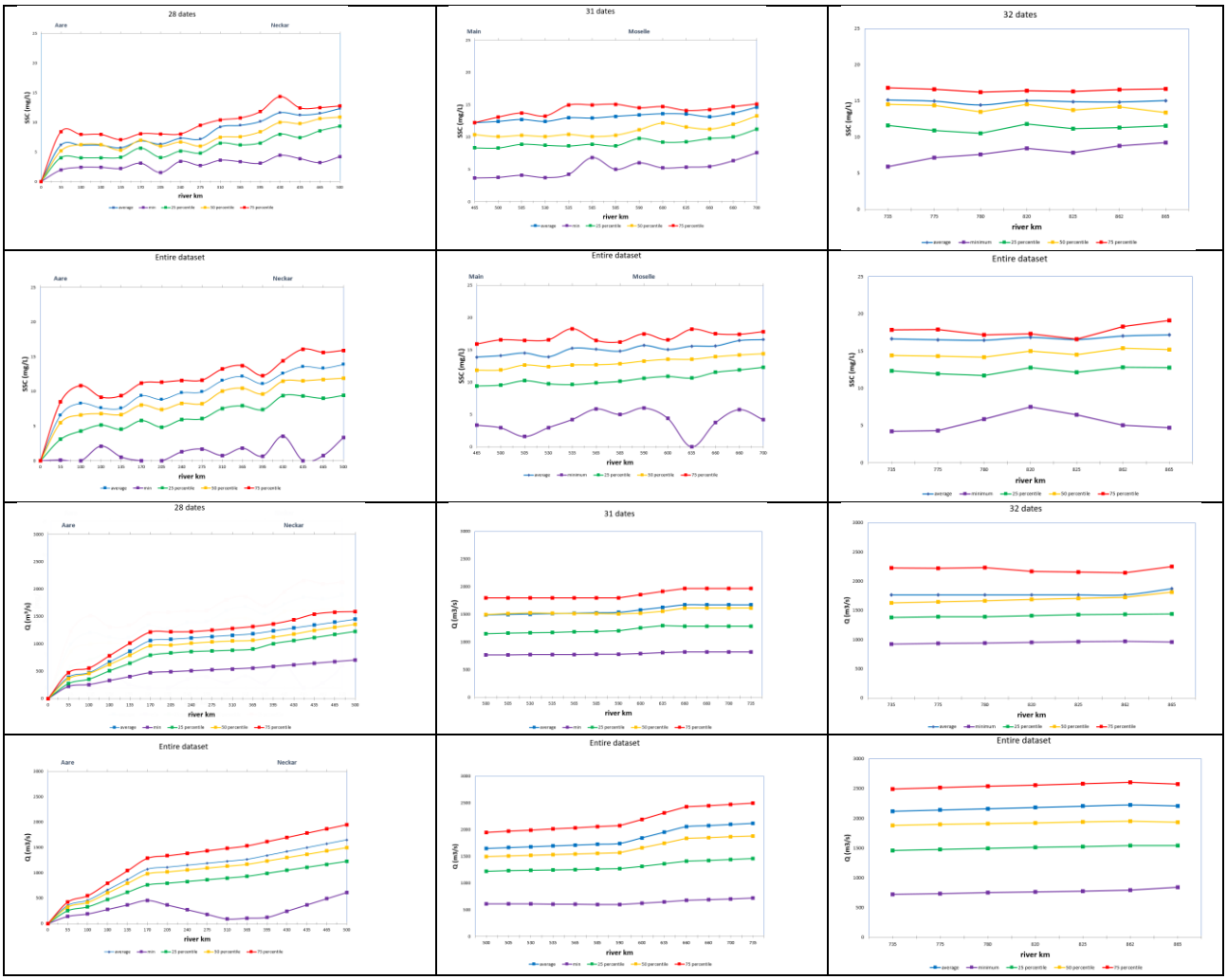

Fig. 3.3. Spatial variation of suspended sediment and discharge

b. Discharge

The sediment transport shows a strong correlation with discharge, as revealed by the pattern in the changes of discharge at every reach. A 4%-fold increase of discharge (averaged over all measurements sites) leads to an 8%-fold increase of SSC change. The SSC change, therefore, becomes relatively more important during periods of high discharge. The concentration of the SSC at Rhine River increases as the discharge also increases; however, the concentration of the sediment depends on whether the discharge is increasing or decreasing and also on the availability of supplies. This is explained further in the next chapter.

c. Cumulative distribution

Cumulative distribution plots are commonly used to illustrate how samples vary among other samples in the river. Fig 3.4 presents the cumulative distribution of SSC in Koblenz Mosel. The plot shows the distribution SSC between selected dates (31 dates) and the entire dataset. Below shows that 70% of SSC are dominant with range of 10-20 mg/L, 20% are with the range 5-10%, and 10% are with the range more than 20 mg/L. Both selected dates and entire dataset

have a similar pattern which shows the selected dates sufficiently represent the distribution of entire dataset.

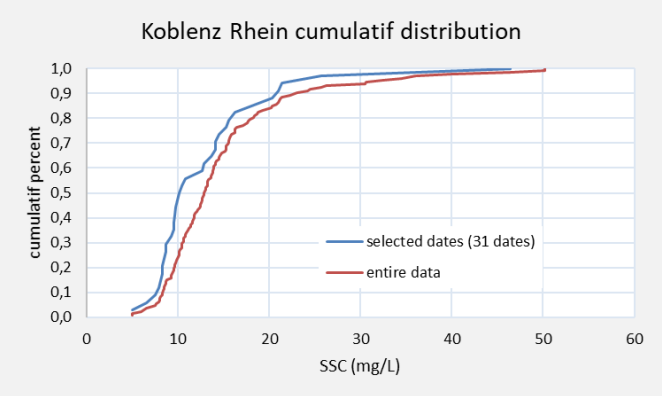

Fig. 3.4. Cumulative distribution of SSC in Koblenz Mosel

3.3.2 Seasonal changes

Daily mean SSCs for six monitoring stations and seven tributaries stations show a clear seasonal variation (Fig.3.5). The seasonal variation of SSC for all monitoring station exhibits a similar pattern, except Rekingen. Rekingen is located in High Rhine, 90.7 km upstream from the Alpine Rhine, presents a high value of SSC in winter and a low value in summer, with the maximum of 15.77 mg/L occurring in January and a minimum of 5.78 mg/L in June. However, SSC has a reverse pattern to discharge, which has a high discharge in summer and low discharge in winter. This must be due to the snowmelt in summer that is the primary water source of the Alpine Rhine and High Rhine. Consequently, high discharge occurs between May and August with discharge peak in June at approximately 663.3 m^3/s and minimum typically occur in January at 352 m^3/s. The different pattern between SSC and discharge can be concluded that SSC remains low during high discharge condition which the water from Alpine Rhine and snowmelt bring an acceptable water quality at Rekingen.

As a whole basin, the SSC in the Rhine River monitoring stations shows the same characteristic of seasonal variation. The monitoring stations Weil Am Rhein, Lauterbourg, Koblenz Rhein, and Lobith show high SSC in winter and low SSC in summer. However, another result shows that the SSC tends to be high in June at almost all monitoring stations where the discharge is minimum. Accordingly, this was probably due to a result of tributaries input that is explained later.

Looking further at tributaries, SSC is higher in the winter and lower in the summer at the Aare River, the Neckar River, the Main River, and the Moselle River. SSC at the Aare River is strongly influenced by the power production where nine power plants and 7 reservoirs found in the headwater (Uehlinger et al., 2009). The reservoir storage let discharge and SSC to release strongly in the winter and decrease in the summer. This process will enhance the seasonal pattern of discharge and SSC. Similar to the Neckar River, the Main River is one of the Rhine tributaries which provides large influence on higher SSC in Rhine River. SSC of the Main River is maximum in January and minimum in May. The ratio between low discharge to high discharge is relatively high with approximately 1:2,5 which high discharge in the winter enhanced increased a high SSC to Rhine River. The differences in SSC magnitude are insignificant for each month at the Moselle River. This is probably due to the construction of 28 weirs with lock, which maintains the amount of water passing through the DAM. Along the Middle Rhine, a smaller tributary the Nahe River joins Rhine River. At the confluence of this

reach, the daily SSC and discharge are maximal in February (25 mg/L) and minimal in June (16 mg/L). Another tributary that gives a smaller impact of the Lower Rhine is the Ruhr River (Q mean= 69.8 m^3/s). Impact on the increases of SSC depends on discharge. However, discharge is not the direct control on SSC, but provides a surrogate for the turbulence forces suspending the sediment. The evidence suggests that great turbulence as the discharge rises correlated with the larger discharge allows the higher load of sediment to be held in suspension. SSC data are missing for November to December because of the higher cloud cover in winter resulting in fewer acquisitions were available.

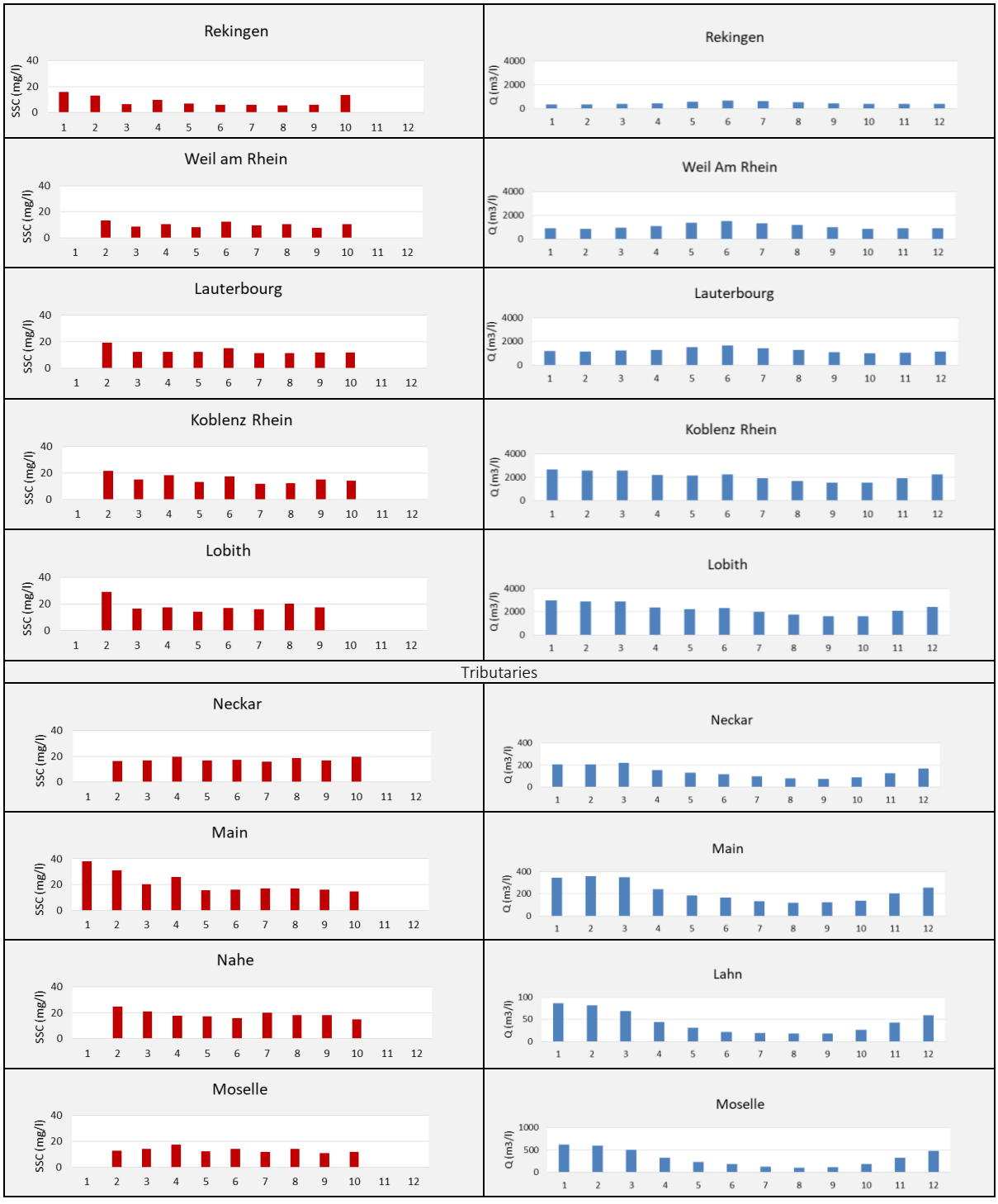

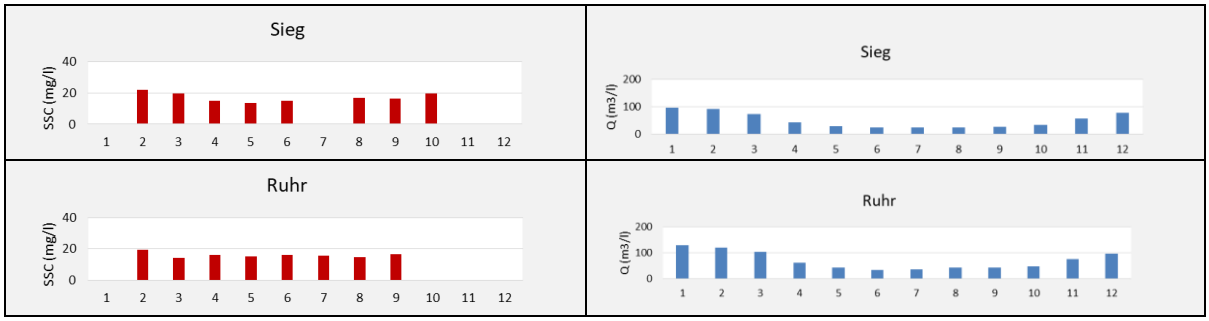

Fig. 3.5. Seasonal variation of SSC in Rhine River average monthly SSC for the 1995 -2016 period

3.4 Suspended sediment concentration transport dynamics

The suspended load usually consists of finer particles, such as silt and clay. SSC is generally several orders of magnitude below its sediment transport capacity (Knighton, 1998). Therefore, the rate of supply is a dominant control of SSC. Fig 3.6 shows the hydrograph of discharge and SSC. Hysteresis occurred when the supplied sediment is higher during the rising limb compared to the falling. The sediment deposited and stored on the channel between storms is entrained by the rising velocity during the rising limb, leaving less sediment supplied to the flow during the falling limb.

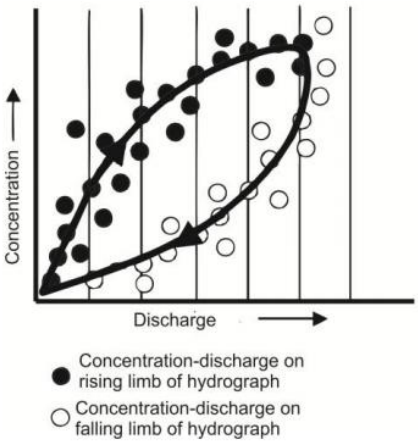

Fig. 3.6. Generalized hysteresis curve for SSC showing the rising limb of the hydrograph with the higher concentrations than the falling limb (Burge, et al., 2014)

3.4.1 Tributaries characteristics

Fig 3.7 a-b-c- show SSC characteristics of tributaries for the period 1995 to 2016. Among tributaries, the daily average SSC series for the Rhine River revealed that the highest contribution of SSC occurs at the Nahe River (19.2 mg/L), the Main River (18.5 mg/L), and the Neckar River (17 mg/L). In contrast, the Moselle River is recognized as the lowest SSC (13.2 mg/L). A study revealed that the Moselle River was recognized as the primary source of suspended load (the function of discharge and SSC) for the Rhine River since it has the largest discharge among tributaries (Sutari, 2018). However, this study suggests that the Moselle River contribute the least the amount of SSC to Rhine River.

A closer inspection of SSC and discharge relation of tributaries becomes particularly manifest at low discharges. Fig 3.7 a-b implies higher SSC at the Nahe River, the Sieg River, and the Ruhr River corresponds for low discharge and low SSC at the Moselle River corresponds for high discharge. However, the high variability in SSC led to the analysis on longer timescales and stratification of data to attempt to describe the high and low SSC values. Meanwhile, under high discharge condition, the Moselle River gives the most significant contribution of SSC to the Rhine compared to other tributaries due to owing a high discharge.

a

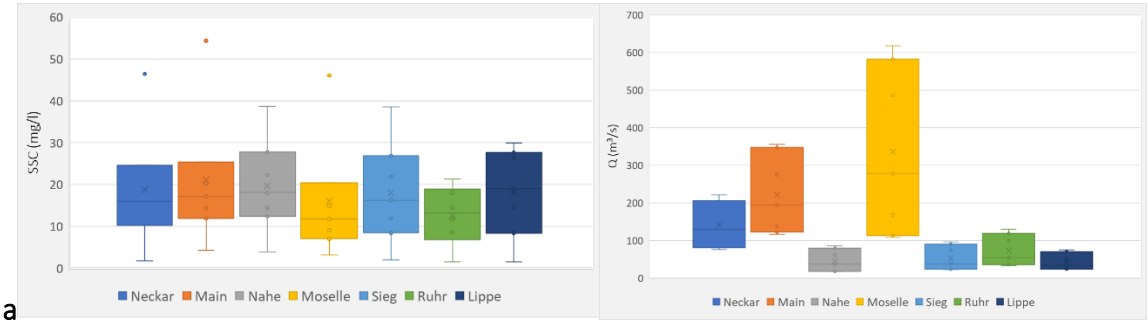

b

	Neckar	Main	Nahe	Moselle	Sieg	Ruhr
average SSC (mg/l)	17,0	18,5	19,2	13,2	17,0	14,9
min SSC (mg/l)	1,7	4,3	3,9	3,1	2,0	1,4
max SSC (mg/l)	46	54	39	46	39	29
catchment area (km³)	13957	27140	4039	28152	2832	4427
n (total data)	276	240	232	120	125	165

c

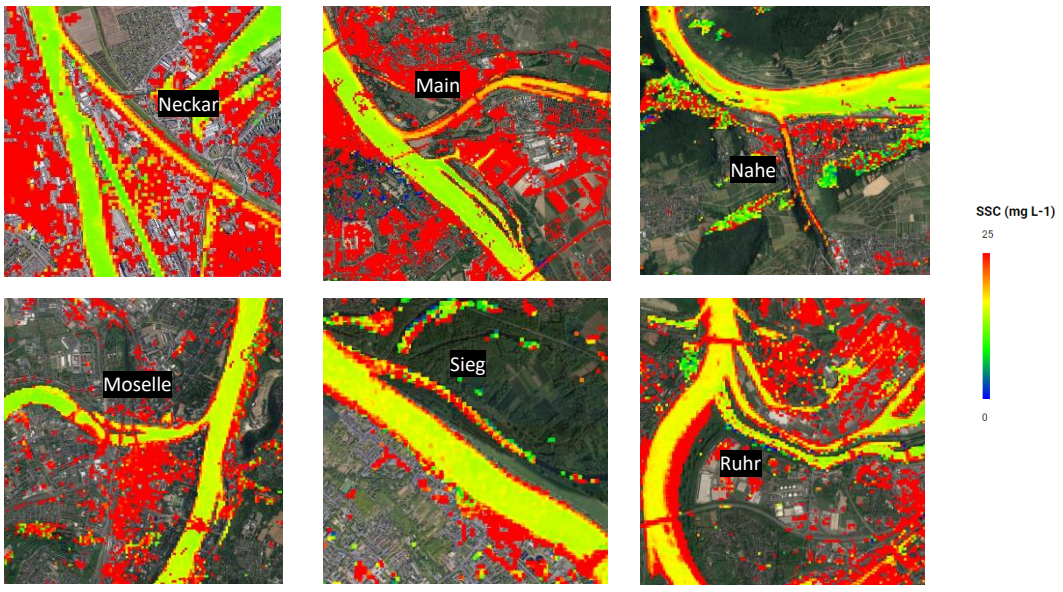

Fig. 3.7. Average of SSC at Rhine tributaries. The SSC is calculated from the model using data from 1995 to 2016.

3.4.2 Sediment supply changes

The change of SSC is represented in three hydrology conditions, which are high discharge, moderate discharge, and low discharge. There are one case of SSC under high discharge, three moderate discharge, and one case of SSC under low discharge. Other cases are presented in the *Appendix*.

Extreme examples of flood peak and increased SSC is illustrated during a flash flood on 13-03-2006 showing a *clockwise* loop. Under high discharge condition, an event shows an extremely increased range SSC from 14.78 to 54.20 mg/L. High discharge was at the beginning of the first hysteresis loop (e.g. first flushes) that could be the reason high magnitude of SSC (Fig.3.8 c-d). Moreover, SSC typically increased downstream when tributary sources flash flood enters the Rhine River (Fig. 3.8 a). The SSC arose significantly on 13-03-2006 after tributaries confluence of Rhine River, such as at the Neckar River (2.5 mg/L), at the Main River (7.6 mg/L), and the Moselle River (12.5 mg/L). Since limited daily data available, the temporal hydrograph-sediment graph and hysteresis pattern were studied only at Lobith.

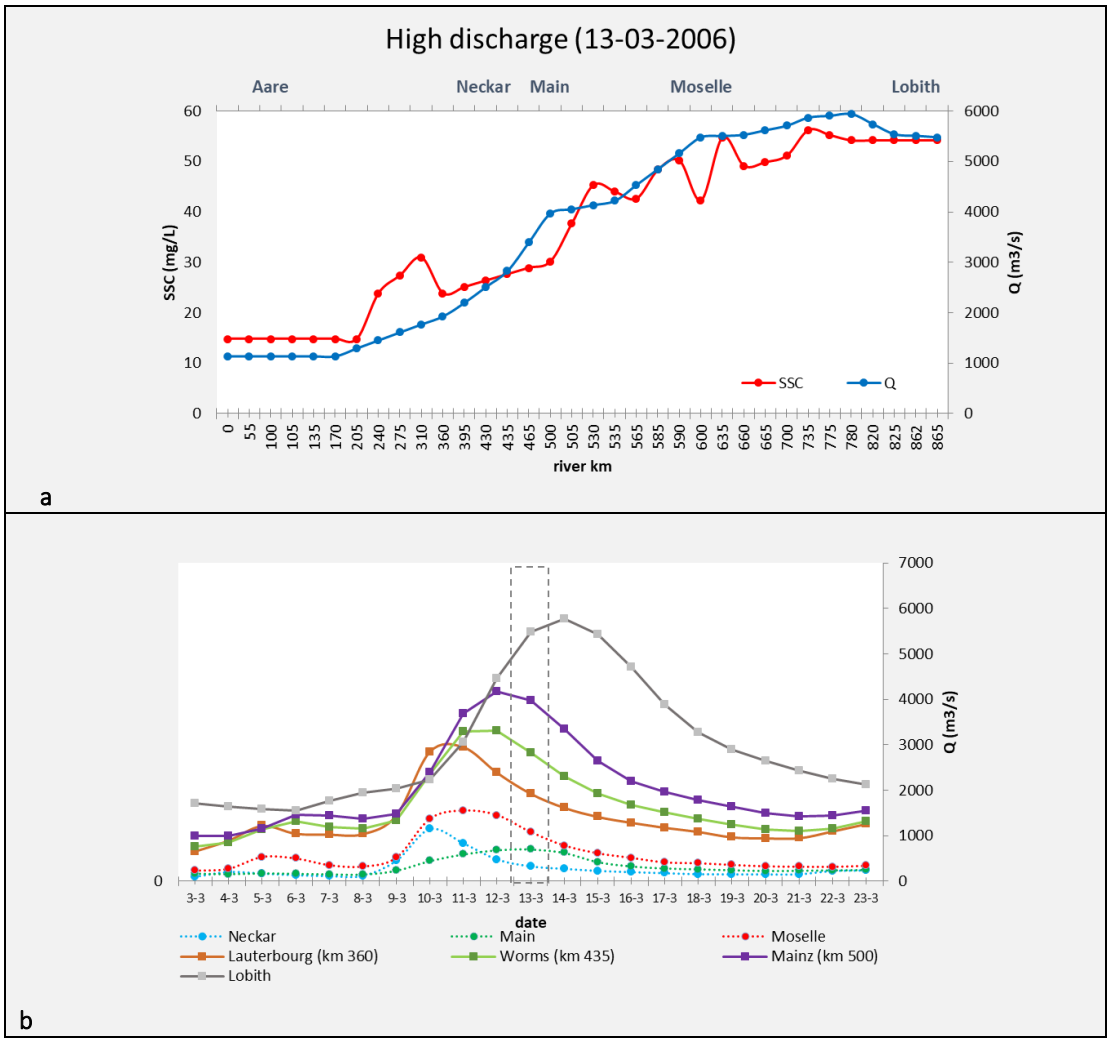

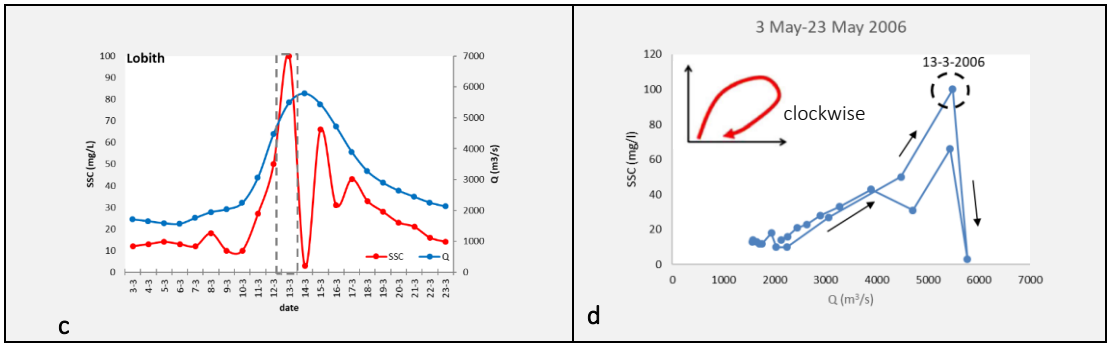

Fig. 3.8. (a) Spatial analysis of SSC from upstream to downstream (b) Temporal hydrograph for several locations and tributaries (c) Hydrograph and sediment graph of events at Lobith, the dashed line indicates the preference date of event (d) Corresponding analysis of hysteresis pattern on **13-03-2006**

The above example explains how the significant magnitude of SSC can be influenced by a high discharge event (flood). However, another result demonstrates moderate flow corresponds to considerable increased of SSC which represented as a *figure-eight* loop (Fig.3.9). On 21-09-2006, the SSC arose from 17.58 to 40.56 mg/L from upstream to downstream. Tributaries such as the Neckar River, the Main River, and the Moselle River contributed SSC to Rhine River by 4.16 mg/L, 3.12 mg/L, and 2,68 mg/L respectively.

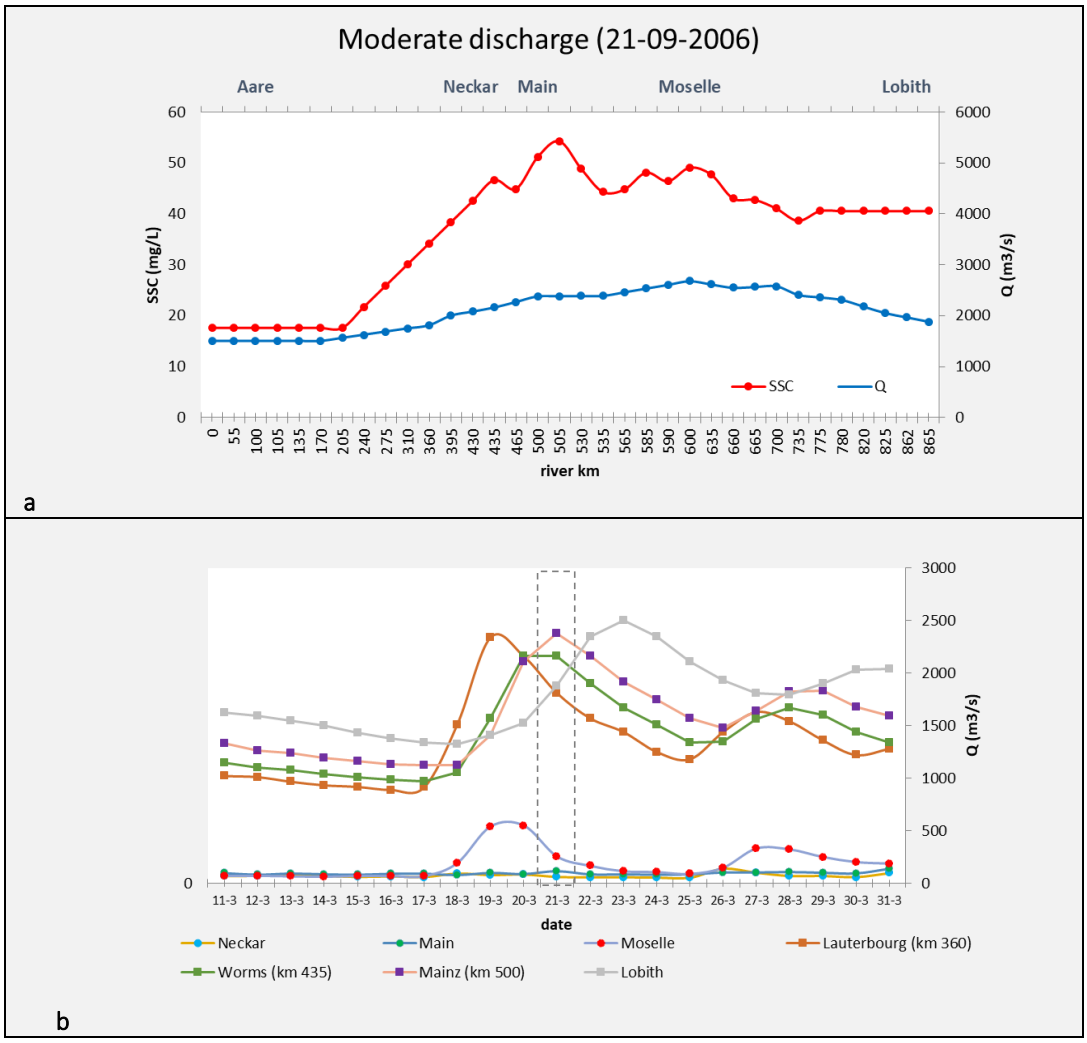

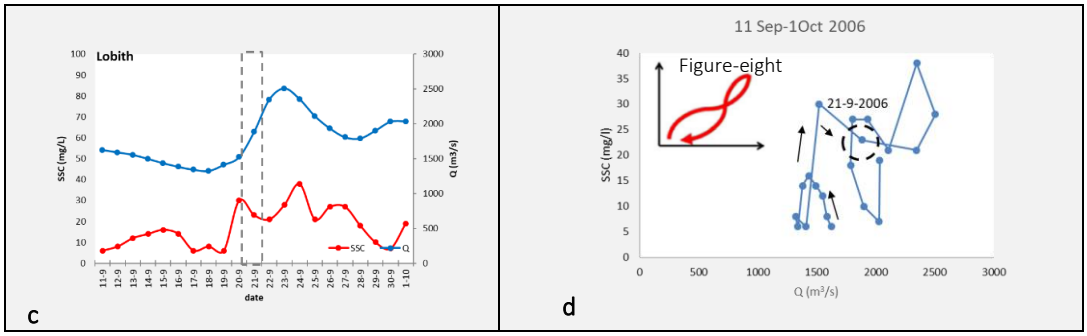

Fig. 3.9. (a) Spatial analysis of SSC from upstream to downstream (b) Temporal hydrograph for several locations and tributaries (c) Hydrograph and sediment graph of events at Lobith, the dashed line indicates the preference date of event (d) Corresponding analysis of hysteresis pattern on **21-09-2006**

Other results showed on *counterclockwise* loop (Fig.3.10 & 3.11) which occurred on moderate discharge, such as on 21-03-2009 and 03-03-2011. On 21-03-2006 and 03-03-2011, the SSC arose from 7.78 to 24.03 mg/L and 7.59 to 14.19 mg/L respectively from upstream to downstream. On 21-03-2009, the Neckar River and the Main River contributed to a higher SSC to Rhine River by 4.16 mg/L and 3.12 mg/L respectively than the Moselle River by 2,68 mg/L (Fig.3.10a). In contrast, the Moselle River contributed the higher SSC by about 4.57 mg/L than the Neckar River (2.96 mg/L) and the Main River (1.86 mg/L) on 03-03-2011 (Fig.3.11a).

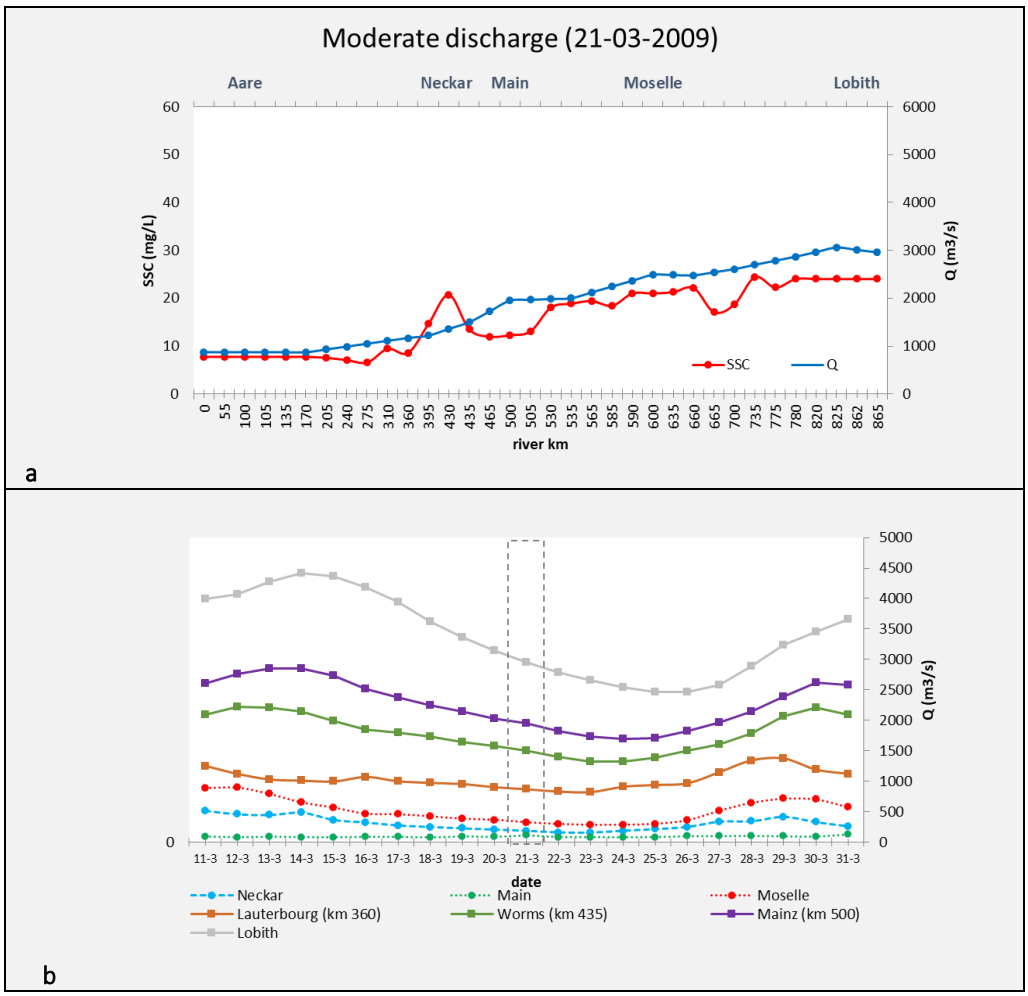

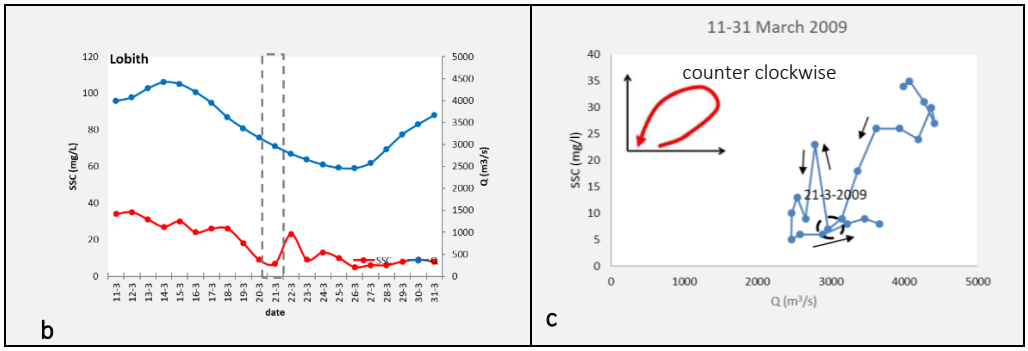

Fig. 3.10. (a) Spatial analysis of SSC from upstream to downstream (b) Temporal hydrograph for several locations and tributaries (c) Hydrograph and sediment graph of events at Lobith, the dashed line indicates the preference date of event (d) Corresponding analysis of 21-03-2009

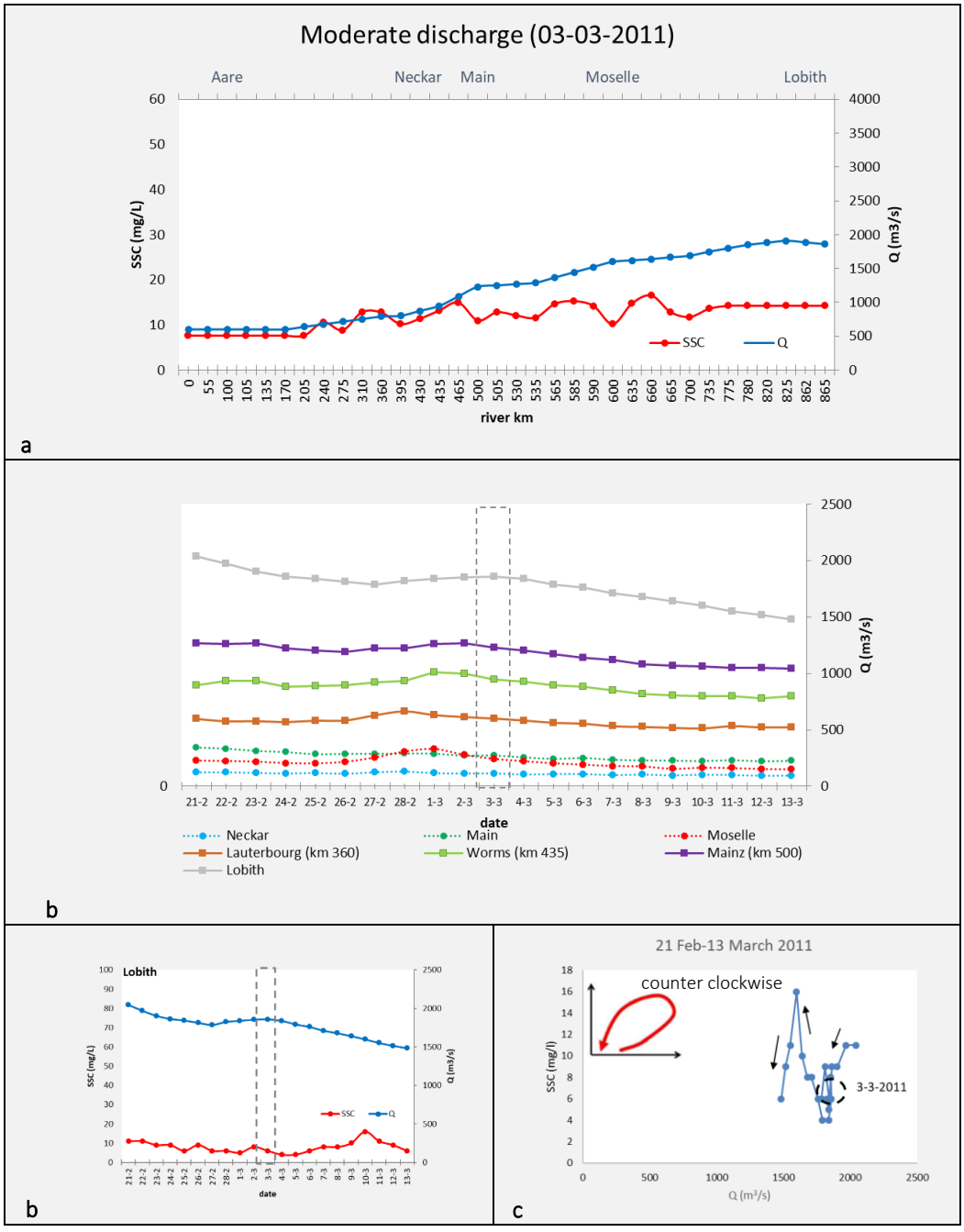

Fig. 3.11. (a) Spatial analysis of SSC from upstream to downstream (b) Temporal hydrograph for several locations and tributaries (c) Hydrograph and sediment graph of events at Lobith, the dashed line indicates the preference date of event (d) Corresponding analysis of 03-03-2011

Turning to low discharge condition, the SSC remained low following the discharge pattern for almost all cases, on 5-8-2015 presented by a higher SSC from 7.54 to 13.13 mg/L (Fig.3.12a). During the low discharge condition, the increased of SSC was almost equal from upstream to the downstream area. The upstream tributaries input such as the Neckar River (1.35 mg/L), the Main River (0.54 mg/L), and the Moselle River (0.84 mg/L) contributed to almost equal SSC by respectively.

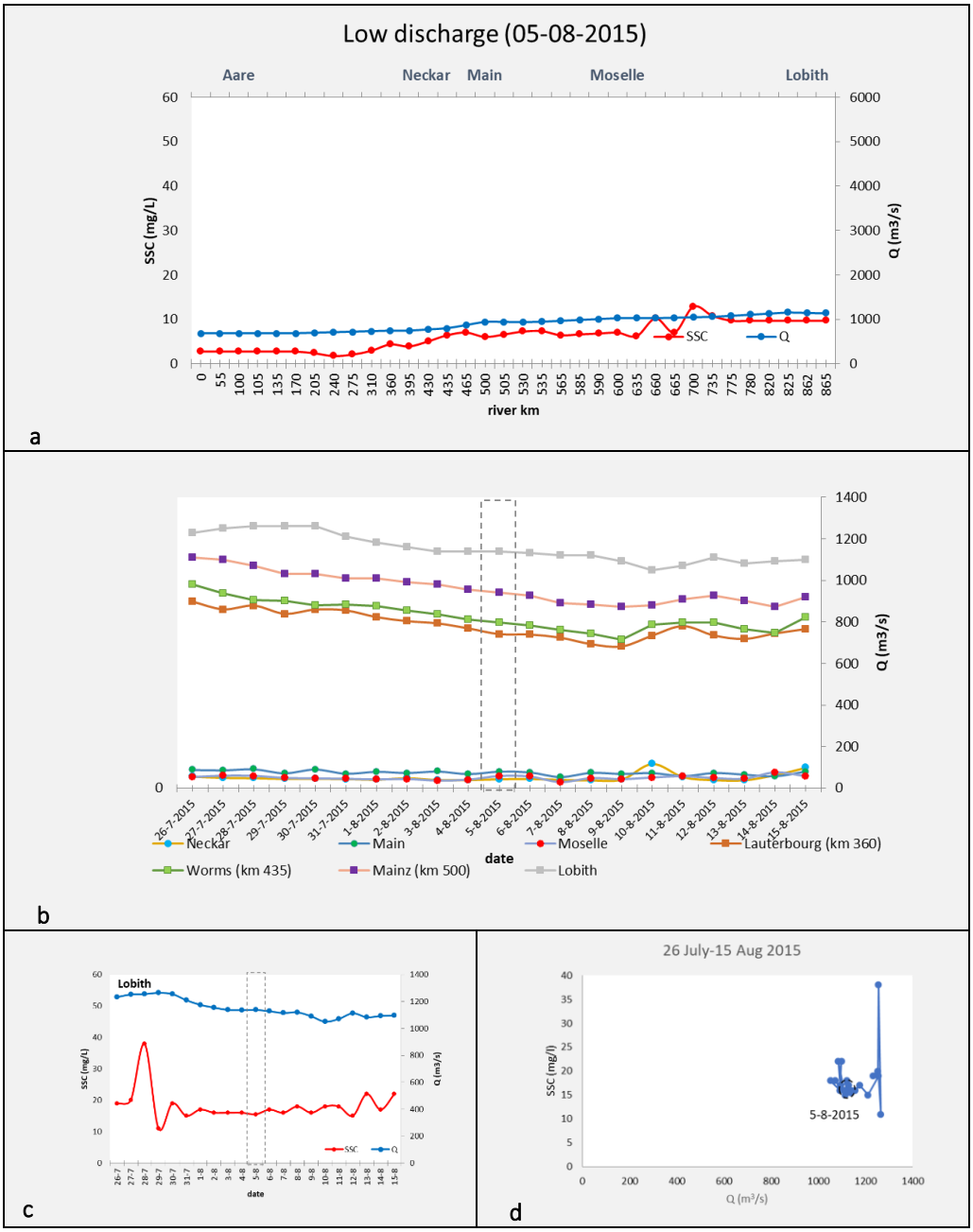

Fig. 3.12. (a) Spatial analysis of SSC from upstream to downstream (b) Temporal hydrograph for several locations and tributaries (c) Hydrograph and sediment graph of events at Lobith, the dashed line indicates the preference date of event (d) Corresponding analysis of 5-8-2015

4. DISCUSSION

4.1 Suspended Sediment Concentration Transport Dynamics, Mechanics, and Sources Under Different Hydrological Conditions

The mechanism underlying suspended sediment transport during different hydrological conditions are characterized by hysteresis patterns. These differences in hysteresis pattern are due to the different sources of supply in different parts of the study area. The hysteresis and sediment graph plots during different events vary in this study, but there are some general (typical) cases.

The *clockwise* loop was represented during a series of flash flood on 13-03-2006 at Lobith; the flood came from upstream and several tributaries. Marked increase of SSC that can be caused by high discharge condition or in this term 'flood' can make up a large contribution of the sediment delivery. In this event, the sediment is easily eroded and transported downstream resulting outwash sediment stocks from the channel without any sediment replenishment.

The *clockwise* loops in previous studies have been interpreted to suggest that a sufficiently high discharge is able to mobilize nearby sources of sediment (along the channel and on nearby fields) and that these sources are exhausted on the rising limb of each storm hydrograph (De Girolamo et al., 2015; Francke et al., 2014; Sun et al., 2016; Tena et al., 2014; Jeje et al., 1991; Asselman & Middlekoop, 1998). However, Steegen et al. (2000) suggested that *clockwise* hysteresis was produced not by sediment flushing and exhaustion, but by the supply of sediment from distant hillslope sources. In this scenario, the sediment from sources close to Lobith reached quickly and was less likely to be deposited, producing a sediment peak that preceded the discharge peak. This study confirms Steegen et al.'s (2000) result that the SSC is certainly high as an early stage of the flood event, meaning that there is enough available sediment in the water, although the latter event had a larger discharge. The availability of large amounts of sediments from tributaries supports the idea that the sediment which had been stored in the channels was being exhausted. SSC at Lobith increased linearly with the increasing discharge to downstream (Fig.3.8 a); however, the highest increased SSC is originated from the Moselle River, and followed by at the Main River, and at the Neckar River. Therefore, major sources of SSC at Lobith was mostly regulated by the River Moselle in high discharge condition. As already explained in the previous chapter, under high water condition, the Moselle River gives the most significant contribution of SSC to the Rhine compared to other tributaries owing to a high discharge. The evidence suggests that great turbulence as the discharge rises correlated with the larger discharge allows the higher load of sediment to be held in suspension.

Turning to moderate discharge condition, *figure-eight* loop on 21-06-2009 characterized by a *clockwise* loop at high discharges and *counter-clockwise* loop at low discharges indicates that SSC was higher earlier on the rising limb hydrograph than the discharge event. Interestingly, although the discharge is categorized as moderate, the increased SSC is remarkable mainly on tributaries confluence. There was a significant increase of SSC after the Neckar River and the Main River joined the Rhine River. This implies that the upstream tributaries input such as the Neckar River and the Main River contributed to major sources of SSC to the downstream in moderate discharge condition. However, there was no significant increase of SSC after the Moselle River joins the Rhine River. Fig 3.9 b shows clear evidence that the contribution of SSC

from the River Moselle is less due to the timing of sediment supply (SSC is assumed to be linear with discharge) by the Moselle River was relatively early (two days before), resulting in less SSC being transported on 21-06-2009. This study captures the probability of deposition, however, it increases with the travel time to downstream. Further analysis on hydrograph shows that the Main River and the Neckar River reached its peak one day before. This support the idea that the considerable increase of SSC at Lobith was mostly regulated by the **Neckar River and Main River** in a moderate discharge condition. The increase of SSC was affected by the exhaustion of the SSC in the channel and the travel time of sediment supply from the tributaries. The previous study suggested that this type of pattern has been attributed to a second pulse of sediment input caused by, for example, bank failure or river bed erosion (Fan et al., 2012), or sediment that originates from a distant source (Heidel, 1956). However, bank failure has not been found for this study.

Another result in moderate discharge condition, *counter-clockwise* loop on 21-03-2009 and 03-03-2011, indicates that the peak SSC was delayed and continued to be high after an initial drop, while the discharge decreased (Fig. 3.10 b c & Fig. 3.11 b c). The increase of SSC for the later discharge event suggests that the supply of the suspended sediment during this event was mainly supplied by temporary storage of SSC occurs either in the Rhine upstream or from the tributaries input. Another case, the increase of SSC after an initial drop while the discharge decreases on 3-3-2011 suggests that the sediment is supplied from the tributaries. It was found that the sources of SSC were mainly from the **Neckar River and Main River** from the longitudinal spatial analysis of SSC. Fig 3.11b shows further explanation performed with less contribution of the Moselle River to the increase of SSC at Lobith due to an earlier lead time of sediment supply by the Moselle River (2 days before), resulting in less SSC being transported on 21-06-2009.

Previous studies have been interpreted to suggest *counter-clockwise* loop patterns, in which the increase in SSC is delayed, and it is typically explained by the sediment being supplied from more distant sources (associated with extended travel times), channel bed erosion or prolonged erosion processes during extended storm events (De Girolamo et al., 2015; Fan et al. , 2012; Fang et al., 2015), when the valley slopes form the most important sediment source (Kurashige, 1994), or high rate of bank collapse just after the passage of the flood peak (Ashbridge, 1995). However, this study is in a good agreement with two of these results, which explained that the increase of SSC on a *counter-clockwise* loop is due to the sediment supplied by a distant source (tributaries input) and channel bed erosion or deposition processes.

A pattern defined by no hysteresis loop at low discharges occurred on 5-8-2015 (Fig. 3.12 d). The increase of SSC was almost equal from upstream to the downstream area. This type of hysteresis occurred relatively often during summer and SSC peak simultaneously, which suggest that Q–SSC relations are more controlled by the entrainment of bed material than the transport of hillslope-derived wash load. Moreover, the upstream tributaries input such as the **Neckar River**, the **Main River,** and the **Moselle River** contributed to almost equal amounts of SSC to the downstream. Similar result from Asselman (1999) agreed that no hysteresis often occurs when the rivers—the Neckar River, the Main River and the Mosel River supply almost equal amounts of sediment. Further analysis (in Chapter 3.1.1) showed that among tributaries, the daily average SSC series for the Rhine River revealed that the contribution of SSC is higher at the Main River and the Neckar River than the Moselle River in low discharge condition. The Moselle River contributes the least amount of SSC to Rhine River although owing to a high discharge.

4.2 Factor Affecting Changes in SSC

4.2.1 Travel Time Analysis

The shape of the hysteresis loops is not only affected by exhaustion of the SSC in the channel, but also the travel time of sediment supply from the tributaries. The earlier and later events of the discharge and SSC (hydrograph and sediment graph) show further evidence for the change in the character of sediment transport. Temporal hydrograph shows the relationship between the low and peak discharge event. Since there is a limitation in the SSC model due to Landsat temporal resolution, the SSC is assumed to increase linearly with the discharge for the temporal hydrograph analysis.

Fig.3.8 indicates that the early SSC on high discharge condition (13-03-2006) from tributaries may influence *clockwise* hysteresis loop at Lobith. The discharge reached its maximum at Lauterbourg and the Neckar River on 10-3-2006; at Worms, Mainz and the Moselle River on 12-03-2006; and reached its peak on 14-03-2006 at Lobith. The discharge reached its peak on 14-03-2006 and the maximum SSC reached its peak one day before (13-03-2006) at Lobith. The early sediment supplied by the Moselle River which reached its discharge peak two days on 11-03-2006 provides the evidence for the peak SSC on 13-03-2006 at Lobith. This maximum SSC occurred before the maximum discharge on 14-03-2006, represented in a *clockwise* hysteresis loop (Fig.3.8 d).

Fig.3.11 c-d shows that the late sediment supply by tributaries, such as the River Neckar and the Main River, may result in *counter-clockwise* hysteresis at Lobith. The discharge (3000 m3/s) at Lobith occurred on 03-03-2011. The discharge reached its maximum at Lauterbourg on 28-02-2011; at Worms on 01-03-2011, Mainz on 02-03-2011 and the Moselle River on 01-03-2011; and the Main River and the Neckar River reached its peak on 03-03-2011 (Fig.3.11 b). However, as the timing of sediment supply by the Neckar River and the Main River was relatively late, i.e., after the passage of the flood in the River Rhine, the resulting hysteresis loop is *counter-clockwise*. Therefore, SSC increased, while the discharge decreased when the sediment supplied from the tributaries is available. Further evidence found that the SSC increased in some areas along the channel. This implies that the temporary storage of SSC plays an important role in increasing sediment at Lobith despite the amount of SSC increased considerably mainly from the Neckar River and Main River (Fig.3.11 a).

Exhaustion of SSC is suggested by the travel time between peak SSC and discharge. The travel time for high discharge is consistent one day, while there were 2-3 days for moderate and low discharge conditions. There was a significant correlation which shows that less travel time revealed a positive correlation with high SSC which travels on high discharge. In contrast, the higher travel time indicates the higher dependence of sand entrained from the channel, which could be correlated with moderate discharge and low discharge conditions. This result concurs well with Asselman & Middelkoop's (1999) finding that the travel time between the SSC and discharge peaks is normally within one to three days in the Rhine River.

4.2.2 Reservoir Sedimentation

In the 20th century, the Rhine River was provided with transverse groynes to have better navigability (Buck et al., 1993). Several dams were built for hydropower and navigation purposes in the main channel and its tributaries. The engineering construction leads to a decrease in the bedload, which results in bed erosion. Therefore, fine sediments are supplied

to the river at km 336-338. Other supply sites are located at km 534 and km 582-603 (Frings et al., 2014).

Fig. 4.1 shows volumes of sediment artificially supplied to the river (Frings et al., 2014). The relocation of some of fine-grained sediments would increase the concentration of suspended matter in the Rhine downstream of Iffezheim barrage over many kilometers for a long period. It confirms that bed stabilization will lead to increase the suspended sediment in the Rhine River.

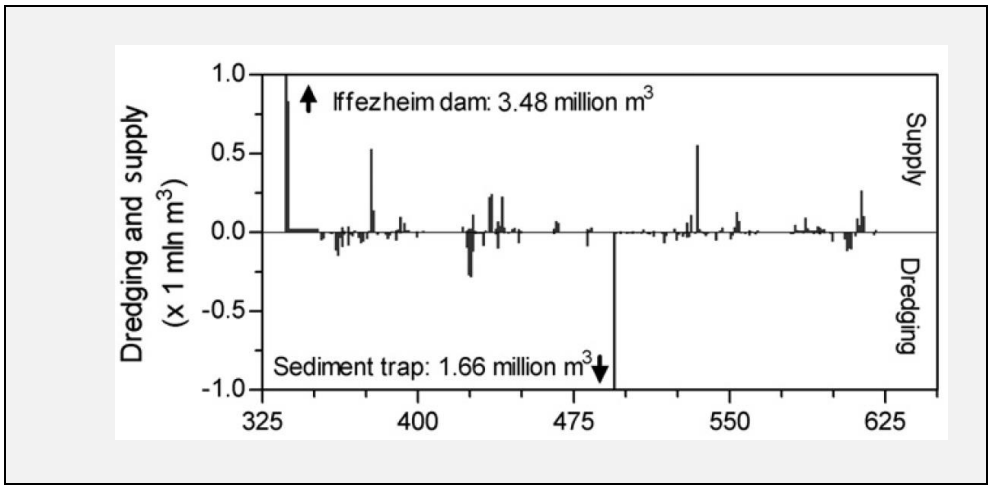

Fig. 4.1. Supply and dredging Rhine River km 325 to km 625 (Frings, et al., 2014)

4.3 Suitability and Uncertainties of Remote Sensing for the Assessment Suspended Sediment

There are several limitations of SSC model that must be considered for analyzing the result. However, Landsat appears to be the most suitable for predicting the SSC in Rhine River since it has a relatively high spatial resolution (30-60m) and long-term data record (>30 years). Although another satellite image such as MODIS produces daily data, small spatial resolution of 250 appears to be not suitable to discriminate SSC particle in the Rhine River (Zheng et al., 2015).

The model is built using remote sensing which has limitations in temporal resolution. Temporal resolution represents the information of date acquisition of satellite and the cloud cover. Each satellite crosses every point on Earth once every 16 days with 8 days offset data acquisition, while two Landsat satellites were in operation. However, the discharge data and SSC used for the regression model are bi-weekly. Therefore, this condition results in only limited satellite images, discharge, and SSC data that correspond each other. Moreover, cloud cover results in worse satellite images quality in the wet season, resulting in the higher error model in the wet season than in the dry season and only limited number of satellite images are used to build the SSC model. As a result, the range of estimated SSC produced by the model is smaller than the range of SSC observed based on *in-situ* measurements/ the entire database. Since only limited range is used, the extreme conditions are probably missing.

The model could only be analyzed for its SSC in 1-2 meter from the water columns and would adjust the result in the shallow water (Markert et al., 2018 and Volpe et al., 2011). To

make the limitation smaller, the model is filtered by only at least 60 m from the channel edge to limit the interference with the channel bottom (Markert, et al., 2018).

The model effectively predicts suspended sediment for values less than 20 mg/L and is estimated with less accuracy above those values (Fig. 3.2). Values are under-estimated constantly at high concentration (>20 mg/L). Of the SSC value, 84% were below than 20 mg/L and 16% were above 20 mg/L. Some studies found that the model that works well at low concentration can saturate to a constant value at higher concentrations (Topliss et al., 1990). Model saturation for high SSC value was probably as a result of a small fraction of data with high SSC values, large variation of maximum and minimum SSC value and processing limitation (Pereira et al., 2018). Landsat images are displayed in integer pixel-format and the number of bits used for the representation limits the maximum pixel value, such as images processing may be likely exceeding their limiting value, causing the pixel to saturate near a constant bit value (Jensen, 2009). Another reason, spectral response for the water can adjust dramatically within a green and red wavelength when the dissolved organic matter concentration and the chlorophyll are high (Jensen, 2009). In contrast, this study shows no discernible pattern in which the spectral band was used among model that saturate. We suggest instead that a large variation of maximum and minimum SSC values may result in saturation at high SSC.

Finally, the differences between the SSC could not be explained in the depth-integrated sediment concentration since the model is represented by a group of pixels. Moreover, in the extreme discharge condition, the bed load transport and other materials in water column might be mixed. Therefore, remote sensing could not describe the process of mixing of SSC from the entire water column (from bottom to top).

4.4 Long-Term Monitoring and Applications

Landsat provides essential information in this study, since it provides the satellite images of relatively high spatial resolution over more than two decades. However, the temporal resolution is not sufficient for daily or weekly observation of SSC in the river, since the data are frequently collected every 14 days and with 8 days offset data acquisition, while two Landsat satellites were in operation.

To build a long-term SSC analysis, other satellite instruments that have better spatial and temporal resolution are required. Furthermore, the SSC model result derived from satellite images could be delivered extensively to users on an operational basis such as web-application. Users then could define a period time of interest, region interest, and seasonal interest. The web-application would let the users receive the SSC for each Landsat pixel in the region of interest from Landsat collection within a selected period. Users could also download the results with the variation of format type such as a graphic/chart or in a table.

Remote sensing was further confirmed to be very useful in establishing a time cost effective method for the routine monitoring of the surface water body. The obtained results in this study are an essential source of information for managers or stakeholders in the assessment, monitoring and sustainable use of surface water resources.

5. CONCLUSIONS

This study demonstrates the variation of SSC in the Rhine River. To summarize, we found that the SSC model works well and shows satisfactory performance. The SSC retrieval model results in a higher R^2, RMSE, and NSE values for 0.43, 11.08 mg/L, and 0.38 respectively in the wet season than in the dry season 0.30, 12.66 mg/L, and 0.29 respectively. Model error statistics such as Nash-Sutcliffe model efficiency coefficient (NSE) and Root Mean Square Error (RMSE) of entire datasets and season variations work well. However, the model produced in the dry season obtains higher error/ bias than in the wet season, which is 1.01 mg/L and -2.60 mg/L respectively. The bias of the model is -0.02 mg/L for the entire datasets, indicating the model performs well in estimating SSC for the overall average. The models effectively predict suspended sediment for values less than 20 mg/L and estimated with less accuracy above those values.

The change of SSC shows a marked increase of about 6 mg/L at Upper Rhine, gradually increase of about 3 mg/L at Middle Rhine, and relative constant at Lower Rhine. SSC increased in the downstream direction, especially at tributary confluence locations. The first sudden jump was identified at Maxau and followed by Neckar at Upper reaches. There was a substantial 20% increase of SSC from Maxau (km 395) to km 430 based on both selected data and entire data calculations. Meanwhile, the Neckar River was found to be less contributing to the increase of SSC, with only 8% calculated from entire data and 8% decrease from the selected date. At Middle Rhine, the Main River delivers substantially, with approximately 1 mg/L for both entire and selected datasets. The transport of SSC from the Moselle River has even increased strongly to about 10% for both datasets. Further downstream, the changes of SSC were much stable and disappeared completely after km 735, without sudden jumps at tributary confluences, where several small tributaries such as the Ruhr River, the Lippe River, and the Sieg River lie at the Rhine River.

Monitoring stations such as Weil Am Rhein, Lauterbourg, Koblenz Rhein, and Lobith show high SSC in winter and low SSC in summer. The evidence suggests that the SSC is highly depended with the discharge, since a high discharge in winter let the sediment to be in suspension. However, another result shows that the SSC tends to be high in June at almost all monitoring stations where the discharge is minimum. Accordingly, this was probably as a result of tributaries input.

The underlying mechanism of suspended sediment transport during different hydrological conditions were characterized by hysteresis patterns. These differences in hysteresis patterns are due to the different sources of supply in different parts of the study area. The availability of large amounts of sediments from tributaries supports the idea that the sediment which had been stored in the channels was being exhausted. The major sediment source SSC at Lobith was mostly regulated by the River Moselle in high discharge condition which shows a *clockwise* loop. Turning to moderate discharge condition, *figure-eight* loop characterized by a *clockwise* loop at high discharges and a counter-*clockwise* loop at low discharges indicates that SSC was higher earlier on the rising limb hydrograph than on the discharge event. The major source of SSC at Lobith was mostly regulated by the Neckar River and Main River in moderate discharge condition due to affected by exhaustion of the SSC in the channel and the travel time of sediment supply from the tributaries. The contribution of SSC from the River Moselle is less due to the timing of sediment supply by the Moselle River was relatively early resulting less SSC being transported to Lobith. Less contribution of SSC from the River Moselle captures the probability of deposition, however, it increases with travel time to downstream. Another result

in moderate discharge condition is as follows, *counter-clockwise* loop indicates that the peak SSC is delayed and continued to be high after an initial drop, while the discharge decreased. The increase of SSC for the later discharge event suggests that the supply of the suspended sediment during this event was mainly supplied by temporary storage of SSC occurs either in the Rhine upstream or from the tributaries input. The major sources of SSC were found to be mainly from the Neckar River and Main River in a moderate discharge condition. No hysteresis loop at low discharges shows that the increase of SSC was almost equal from upstream to the downstream area. This type of hysteresis occurred relatively often during summer and SSC peak simultaneously, which suggests that Q–SSC relations are more controlled by the entrainment of bed material. Moreover, the upstream tributaries input such as the Neckar River, the Main River, and the Moselle River contributed to almost equal amounts of SSC to the downstream

The shape of the hysteresis loops is not only affected by exhaustion of the SSC in the channel, but also the travel time of sediment supply from the tributaries. Exhaustion of SSC is suggested by the travel time between peak SSC and discharge. The travel time for high discharge is consistent one day, while there were 2-3 days for moderate and low discharge conditions. There was a significant correlation which shows less travel time revealed a positive correlation with high SSC which travel on high discharge. In contrast, the higher travel times indicates the higher dependence of sand entrained from the channel which could be correlated with moderate discharge and low discharge conditions. Another reason provides evidence of increased SSC that the relocation of some of fine-grained sediments would increase the concentration of suspended matter in the Rhine downstream of Iffezheim barrage over many kilometers for a long period. It confirms that bed stabilization will lead to increase the suspended sediment in the Rhine River.

REFERENCES

Antonelli, C., Eyrolle, F., Rolland, B., Provansal, M., & Sabatier, F. (2008). Suspended sediment and 137Cs fluxes during the exceptional December 2003 flood in the Rhone River, southeast France. *Geomorphology, 95*, 350-360.

Ashbridge, D. (1995). Processes of river bank erosion and their contribution to the suspended sediment load of the River Culm, Devon', in Foster I. D. L., Gurnell, A. M. and Webb, B. W. (Eds). In *Sediment and Water quality in River Chichester* (pp. 229-245). Chichester: John Wiley and Sons.

Asselman, N. (1999). Suspended Sediment Dynamics in a Large Drainage Basin: The River Rhine. *Hydrological Processes, 13*(10), 1437-150.

Asselman, N., & Middlekoop, H. (1998). Temporal variability of contemporary floodplain sedimentation in the Rhine–Meuse delta, The Netherlands. *Earth Surface Processes and Landfor,, 23*(7), 595-609.

Batalla, R. J. (2003). Sediment deficit in rivers caused by dams and instream gravel mining. Areview with examples from NE Spain. *Revista C&g, 17 (3-4)*, 79-91.

BfG. (1993). *Untersuchung und numerische M odellierung von subaquatischen Dünen im Rhien bei Niederwalluf (Rheingau).* Report BfG-0774, Federal Institute of Hydrology.

Bisantino, T., Gentile, F., & Trisorio, G. L. (2011). Continuous Monitoring of Suspended Sediment Load in Semi-arid Environments. In S. S. Ginsberg, *Sediment Transport.* InTech. Retrieved from http://www.intechopen.com/articles/show/title/continuous-monitoring-of-suspended-sediment-load-in-semi-arid-environments.

Bormann, H., Pinter, N., & Simon, E. (2011). Hydrological signatures of flood trends on German rivers: Flood frequencies,flood heights and specific stages. *Journal of Hydrology, 404*, 50-66.

Bowers, D. G., Braithwaite, K. M., Nimmo-Smith, W., & Graham, G. W. (2009). Light scattering by particles suspended in the sea: The role of particle size and density. *Cont. Shelf Res, 29*, 1748–1755.

Buck, W., Ferkel, K., Gerhard, H., Kalweit, H., Malde, J. v., Nippes, K. -R., . . . Schmitz, W. (1993). *Der Rhein unter Einwirkung des Menschen – Ausbau,Schifffahrt,Wasserwirtschaft.* KHR-Report 1-11.

Burge, L., Guthrie, R., & Chaput-Desrochers, L. (2014). Hydrological factors affecting spatial and temporal fate of sediment in association with stream crossings of Mackenzie gas Pipeline. *Sci. Advis. Sec. Res.*, 1-36.

Chen, B., Xiao, X., Li, X., Pan, L., Doughty, R., Ma, J., . . . Gir, C. (2017). A mangrove forest map of China in 2015: Analysis of time series Landsat7/8 and Sentinel-1A imagery in Google Earth Engine cloud computing platform. *ISPRS Journal of Photogrammetry and Remote Sensing, 131*, 104-120. doi:https://doi.org/10.1016/j.isprsjprs.2017.07.011

Davis, T. E., & McAnally, H. (2010). *Sediment Management Alternatives for the Port of Gulfport, Mississippi.* Mississippi State Universit, Civil and Environmental Engineering Department. Mississippi State Universit.

De Boer, D., & Crosby, G. (1996). Specific sediment yield and drainage basin scale. *Erosion and Sediment Yield: Global amd Regional Perspectives (proceedings of the Exeter Symposium)_* (pp. 333-). Exeter: IAHS.

De Girolamo, A., Pappagallo, G., & La Porto, A. (2015). Temporal variability of suspended sediment transport and rating curves in a Mediterranean river basin: The Celone (SE Italy). *Catena, 128*, 135-143.

Dean, D., Topping, D., Schmidt, J., Griffths, R. E., & Sabol, T. A. (2016). Sediment supply versus local hydraulic controls on sediment transport and storage in a river with large sediment loads. *J.Geophys.Res.Earth Surf*, 82-110.

Dröge, B., Tippner, M., Gölz, E., Schűrg, M., Engel, M., Busch, N., & Műrlebach, M. (1985). *Instruction for bedload and suspended material sampling.* Koblenz, Germany: Bundesanstalt für Gewässerkunde.

Fan, X., Shi, C., Zhou, Y., & Du , J. (2012). Characteristics of flood regime in Ningxia. *Resource Science , 34*(1), 65-73 (in Chineese with English abstract).

Fang, N., Shi, Z., Chen, F., Zhang, H., & Wang, Y. (2015). Discharge and suspended sediment patterns in a small mountainous watershed with widely distributed rock fragments. *Journal of Hydrology, 528*, 238-248.

Fergusson, R. (1986). Rover loads underestimated by rating curves. *Water Resource Research, 22 (1)*, 74-76.

Francke, T., Werb, S., Sommere, E., & López-Tarazón, J. (2014). *Analysis of runoff, sediment dynamics and sediment yield of subcatchments in the highly erodible Isábena catchment, Central Pyrenees, 14*(12), 1909-1920.

Frings, R. (2015). Sand and Gravel on the Move: Human Impacts on Bed-Material Load Along the Lower Rhine River. In *Geomorphic Approaches to Integrated Floodplain management of lowland Fluvial System in North America and Europe.* New York: Springer. doi:10.1007/978-1-4939-2380-9_2

Frings, R. M., Gehres, N., Prommy, M., Middlekoop, H., Schuttrümpf, H., & Vollmer, S. (2014). Today's sediment budget of the Rhine River channel, focusing on the Upper Rhine Graben and Rhenish Massif. *Geomorphology, 204*, 573-587.

Fryirs, K., & Brierley, G. (2013). *Geomorphic analysis of river system: An approach to reading the landscape.* West Sussex: Wiley-Blackwell.

Gholizadeh, M. H., Melesse, A. M., & Reddi, L. (2016). A Comprehensive Review on Water Quality Parameters Estimation Using Remote Sensing Techniques. *sensors, 16*, 1-43.

Gholizadeh, M. H., Melesse, A. M., & Reddi, L. (2016). A Comprehensive Review on Water Quality Parameters Estimation Using Remote Sensing Techniques. *sensors, 16 (1298)*, 1-43.

Gölz, E. (1990). Suspended sediment and bedload problems of the Upper Rhine. *17*.

Google Earth Engine Team. (2015). *Google Earth Engine: A planetary-scale geo-spatialanalysis platform [WWW Document].* Retrieved from http://earthengine.google.com

Guan, M., Ahilan, S., Yu, D., Peng, Y., & Wrigt, N. (2018). Numerical modelling of hydro-morphological processes dominated byfine suspended sediment in a stormwater pond. *Journal of Hydrology, 556*, 87-99.

Hansen, M., & Loveland, T. (2012). A review of large area monitoring of land cover change using Landsat data. *Remote Sensing of Environment, 122*, 66-74.

Heidel, S. (1956). The progressive lag of sediment concentration with flood wave. *Transaction American Geophysical Union, 37*, 56-66.

Jeje, L., Ogunkoya, O., & Oluwatimilehin, J. (1991). Variation in suspended sediment concentration during storm discharges in three small streams in upper osun basin, Central Western Nigeria. *Hydrological Processes, 5*(4), 361-369.

Jensen, J. R. (2009). *Remote Sensing of the Environment: An Earth Resource Perspective (Second Edition).* New Jersey: Pearson Prentice Hall.

Knighton, D. (Fluvial Forms and Processes A New Perspektif). *1998.* London, UK: Arnold.

Kothyari, U. C. (1996). 'Erosion and sedimentation problems in India' in Erosion and Sediment Yield: Global and Regional Perspectives. *236*, 531-540.

Lahlou, A. (1988). 8) 'The silting of Moroccan dams' in Sediment Bud. *174*, 71-77.

Lillesand, T., Kiefer, R., & Chipman, J. (2014). *Remote Sensing and Image Interpretation.* New York,USA: John Wiley & Sons.

López-Tarazón, J., Batalla, R., Vericat, D., & Balasch, J. (2010). Rainfall, runoff and sediment transport relations in a mesoscale mountainous catchment: The River Isábena (Ebro basin). *Catena, 82 (1)*, 23-34.

Markert, K. L., Schmidt, C. M., Griffin, R. E., Flores, A. I., Poortinga, A., Saah, D. S., . . . Ganz, D. J. (2018). Historical and Operational Monitoring of Surface Sediments in the Lower Mekong Basin Using Landsat and Google Earth Engine Cloud Computing. *remote sensing, 10*, 1-19. doi:doi:10.3390/rs10060909

Masek, J. G., Vermote, E. F., Saleous, N. E., Wolfe, R., Hall, F. G., Huemmrich, K. F., . . . Lim, T. -K. (2006). A Landsat surface reflectance dataset for North America,1990–2000. *Remote Sens.Lett, 3*, 68-72. doi:http://dx.doi.org/10.1109/LGRS.2005.857030

Meade, R. H. (1982). Sources, sinks, and storage of river sediments in the Atlantic drainage of the United States. *Journal of Geology, 90 (3)*, 474-487.

Middelkoop, H. (1997). *Embanked floodplains in the Netherlands. PhD thesis.* Utrecht: Department of Physical Geography, Utrecht.

Moriasi, D. N., Arnold, J. G., Van Liew, M. W., Bingner, R. L., Harmel, R. D., & Veith, T. L. (2007). Model Evaluation Guidelines for Systematic Quantification of Accuracy in Watershed Simulations. *American Society of Agricultural and Biological Engineers, 50 (3)*, 885-900.

Nadal-Romero, E., Lasanta, T., Regüés, D., Lana-Renault, N., & Cerdà, A. (2011). Hydrological Response and sediment Production under Different Land Cover in Abandoned Farmland Fields in a Mediterranean Mountain Environment. *Boletín de la Asociación de Geógrafos Españoles, 55*, 303-323.

Nash, J., & Sutcliffe, J. (1970). River flow forecasting through conceptual models: Part 1. A discussion of principles. *Journal Hydrology, 10*(3), 282-290.

Pekel, J., Cottem, A., & Belward, A. (2016). High-resolution mapping of global surface water and its long-term changes. *Nature, 540*, 418-422.

Pereira, L. F., Andes, L. C., Cox, A. L., & Ghulam, A. (2018). Measuring Suspended-Sediment Concentration and Turbidity in The Middle Mississippi and Lower Missouri Rivers using Landsat Data. *Journal of The American Water Resources Association, 54 (2)*, 440-450.

Pham, Q., Ha, N., Pahlevan, N., Oanh, L., Nguyen, T., & Nguyen, N. (2018). Using Landsat-8 Images for Quantifying Suspended Sediment Concentration in Red River (Northern Vietnam). *remote sensing, 10*, 1-19.

Preusser, F. (2008). Characterisation and evolution of the Rhine River system. *Netherlands Journal of Geosciences-Geologie en Mijnbouw, 87*(1), 7.

Qiu, Z., Xiao, C., Perrie, W., Sun, D., Wang, S., Shen, H., . . . He, Y. (2017). Using Landsat 8 data to estimate suspended particulate matter in the Yellow River estuary. *Journal of Geophysical Research: Ocean, 122*, 276-290.

Ritchie, J. C., Zimba, P. V., & Everitt, J. H. (2003, June). Remote Sensing Techniques to Asess Water Quality. *Photogrammetric Engineering & Remote Sensing, 69 (6)*, pp. 695-704.

Ritchie, J., Schiebe, F., & McHenry, J. (1976). Remote Sensing of Suspended Sediment in Surface Waters. *Photogrammetric Engineering & Remote Sensing*, 1539-1545.

Schmidt, M. (2000). *Hochwasser und Hochwasserschutzs in Deutschland vor 1850 – Eine Auswertung alter Quellen und Karten.* München: Oldenbourg-Industrieverlag.

Spreafico, M., & Lehmann, C. (2009). *Erosion, Transport and Deposition of Sediment- Case Study Rhine -.* International Commission for the Hydrology of the Rhine Basin.

Steegen, A., Govers, G., Beuselinck, L., Oost, K., Quine, T., & Rombaut, A. (2000). The use of phoshorus as a tracer in erosion/ sedimentation studies. *The Role of Erosion and Sedimentation Transport in Nutrient and Contaminant Transfer. 263.* Waterloo, Canada: IAHS Publ.

Sun, L., Yan, M., Cai, Q., & Fang, H. (2016). Suspended sediment dynamics at different time scales in the Loushui River, south-central China. *Catena, 136*, 152-161.

Sutari, C. (2018). *Suspended sediment loads in the Rhine – spatial and temporal trends in the past 50 years.* Utrecht: Faculty geoscience, Utrecht University.

Tena, A., Vericat, D., & Batalla, J. (2014). Suspended sediment dynamics during flushing flows in a large impounded river (the lower River Ebro). *Journal of Soils and Sediments, 14*(12), 2057-2069.

Topliss, B. J., Almos, C. L., & Hill, P. R. (1990). Algorithms for remote sensing of high concentration, inorganic suspended sediment. *Remote Sensing, 11 (6)*, 947-966.

Tremolieres, M., Eglin, I., Roeck, U., & Carbiener, R. (1993). The exchange process between river and groundwater on the Central Alsace floodplain (Eastern France). *Hydrobiologia*, 133-148.

Uehlinger, U., Arndt, H., Wantzen, K., & Leuven, R. (2009). Chapter 6-The rivers of Europe. In *Rivers of Europe* (pp. 199-245). Berlin and Dübendorf: Academic Press.

Vermote, E., Saleous, N., Justice, C., Kaufman, Y., Privette, J., Remer, L., . . . Tanre, D. (2002). Atmospheric correction of visible to middle-infrared EOS-MODIS data over land surfaces: Background, operational algorithm, and validation. *J. Geophys. Res, 83*, 97-111.

Vermote, E., Tanre , D., Deuze, J., Herman , M., & Morcrette, J. (1997). Second Simulation of the Satellite Signal in to the Solar Spectrum, 6S: An Overview. *IEEE Trans. Geosci. Remote Sens., 35*, 675-686.

Vollmer, S., & Goelz, E. (2006). Sediment monitoring and sediment management in the Rhine River. *Sediment Dynamics and the Hydromorphology of Fluvial Systems, 306*, 231-240.

Volpe, V., Silvestri, S., & Marani , M. (2011). Remote sensing retrieval of suspended sediment concentration in shallow waters. *Remote Sensing Environment, 115*, 44-54.

Wenka, T. (2009). *Untersuchungen zur langfristigen Lagestabilität der zum bergsenkungsbedingten Sohlausgleich eingebrachten Waschberge im Rheinstrom.* Karlsruhe: AbschlussberichtBundesanstalt für Wasserbau.

Woodward, J., & Foster, I. (1997). Erosion and Suspended Sediment Transfer in River Catchments: Environmental controls,processes and problems. *Geography, 84 (4)*, 353-376.

Yepez, S., Laraque, A., Martnez, J.-M., Sa, J., Carrera, J. M., Castellanos, B., . . . Lopez, J. L. (2018). Retrieval of suspended sediment concentrations using Landsat-8 OLI satellite images in the Orinoco River (Venezuela). *Comptes Rendus Geoscience*, 20-30. doi:https://doi.org/10.1016/j.crte.2017.08.004

Zheng, Z., Li, Y., Guo, Y., Xu, Y., Liu, G., & Du, C. (2015). Landsat-Based Long-Term Monitoring of Total Suspended Matter Concentration Pattern Change in the Wet Season for Dongting Lake, China. *Remote Sens, 7*, 13975-13999.

Zhu, Z., Wang, S., & Woodcock, C. (2015). Improvement and expansion of the Fmask algorithm: cloud, cloud shadow, and snow detection for Landsats 4–7, 8, and Sentinel 2 images. *Remote Sens. Environ, 159*, 269-277.

APPENDIX

Spatial variation of SSC in Rhine River

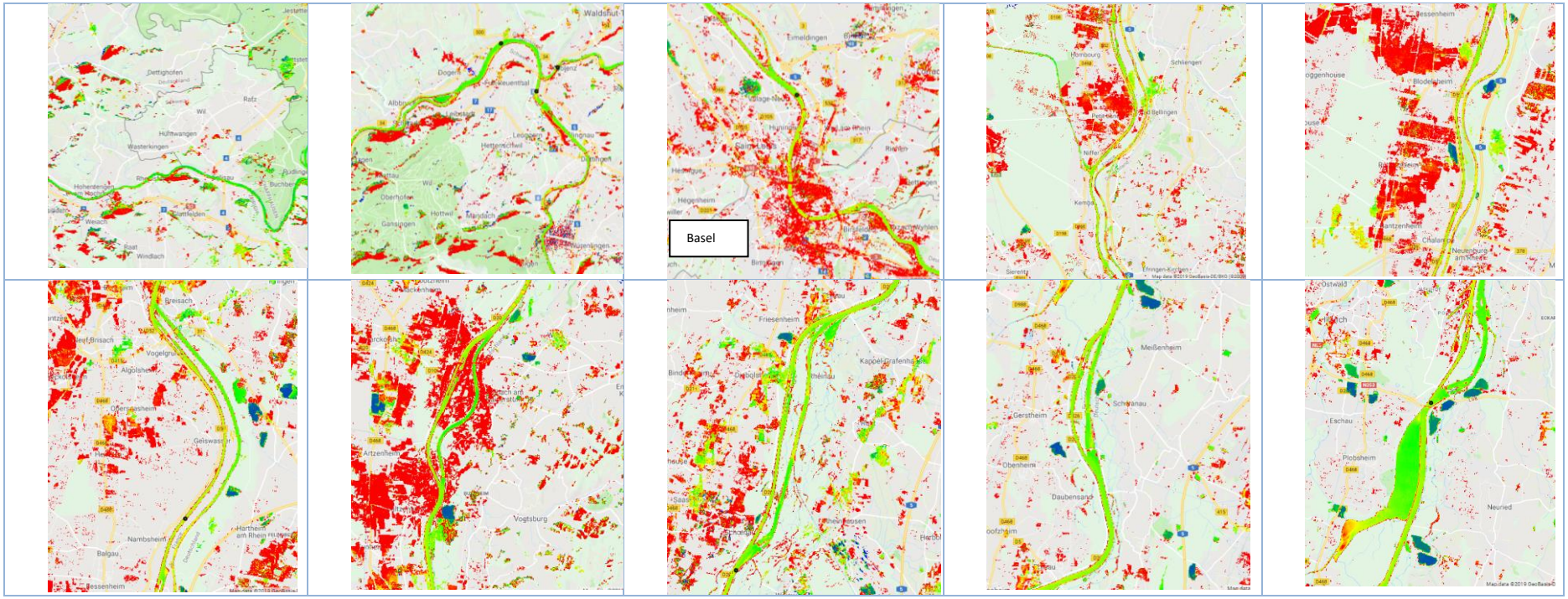

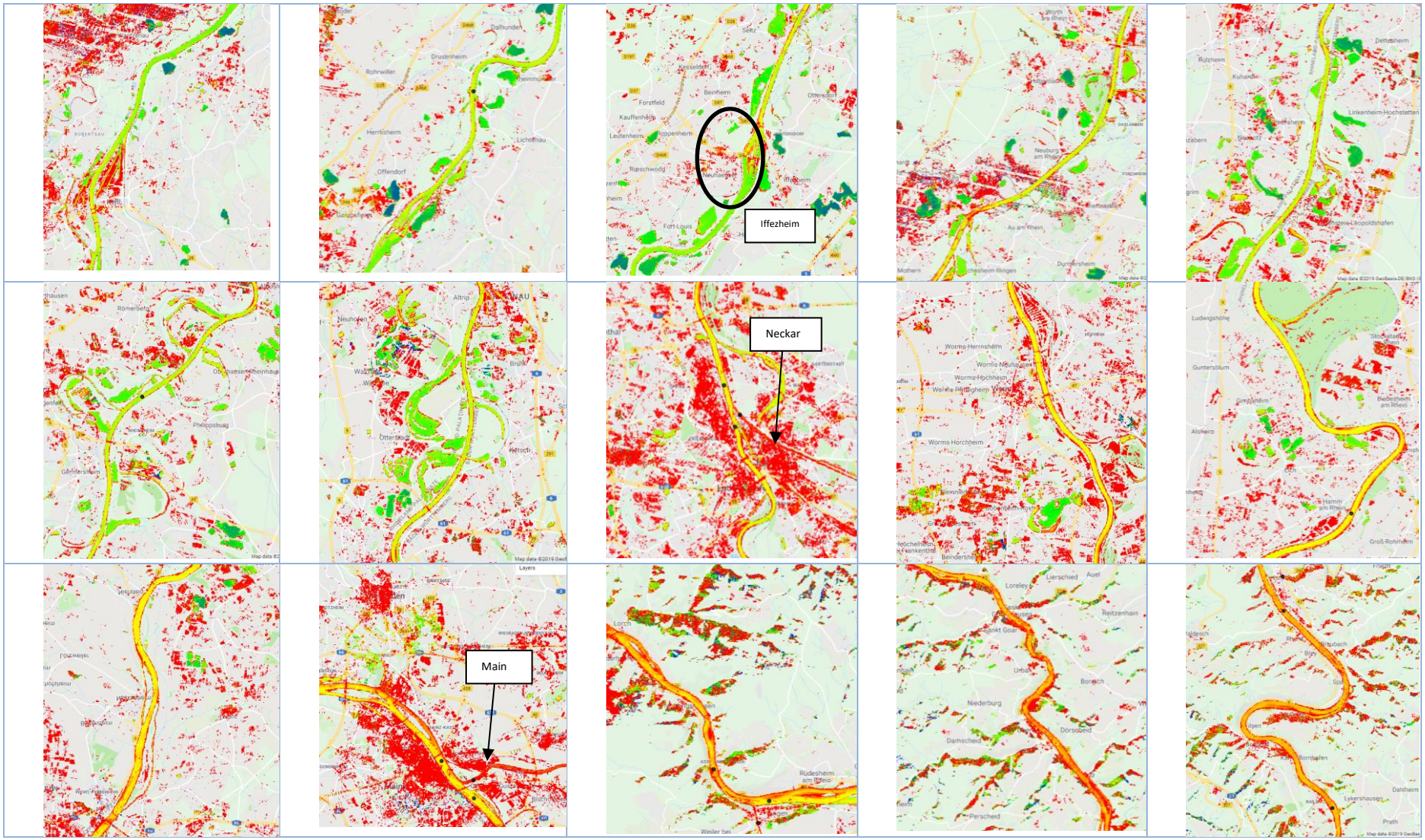
Iffezheim
Neckar
Main

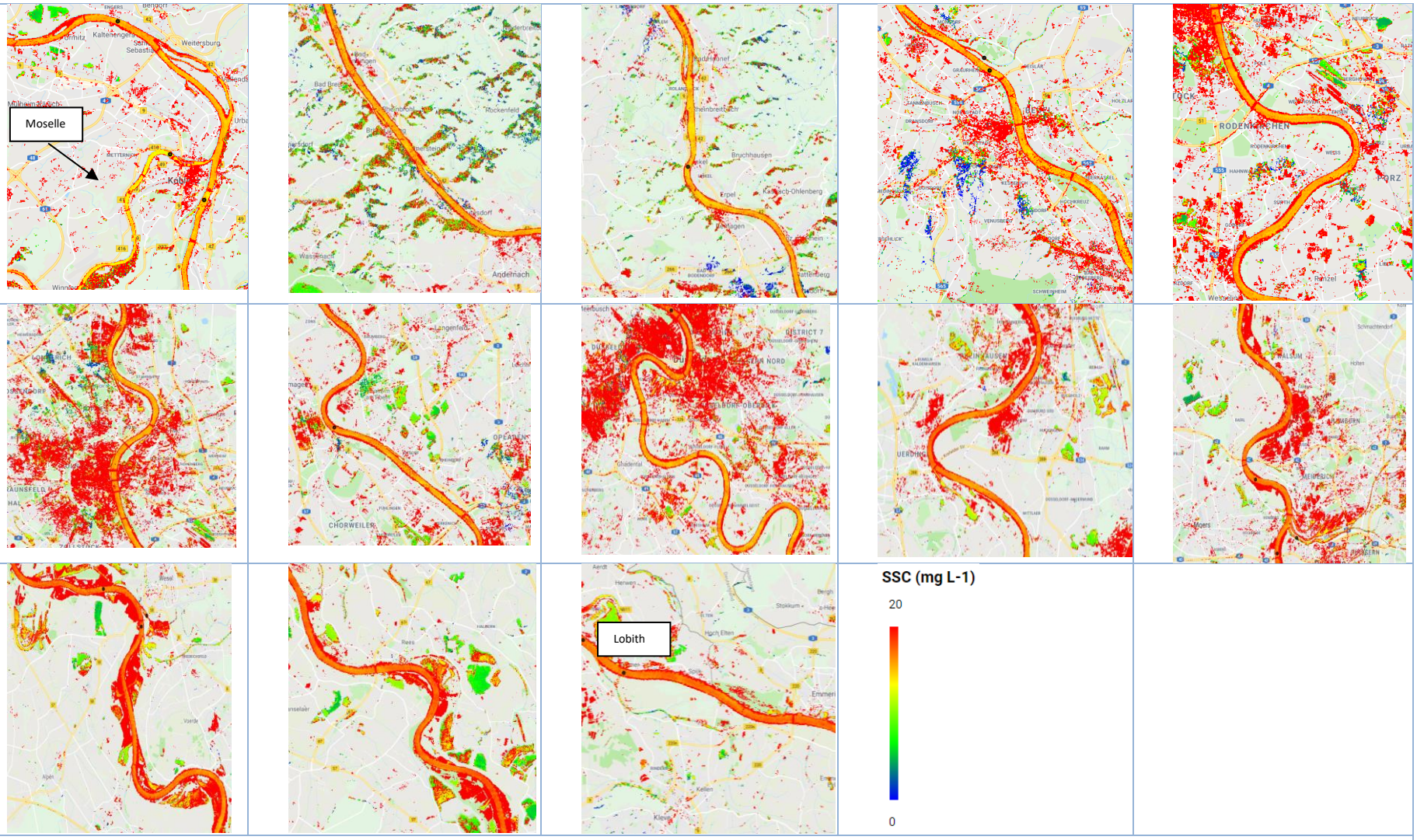

Spatial changes in the mean of SSC from 1995 to 2016 in Rhine River shown by gradual changes in color

A. POTENTIAL SOURCE OF SUSPENDED SEDIMENT IN THE RHINE RIVER BASIN UNDER DIFFERENT CONDITION

1. Suspended-sediment sources under high water & moderate water

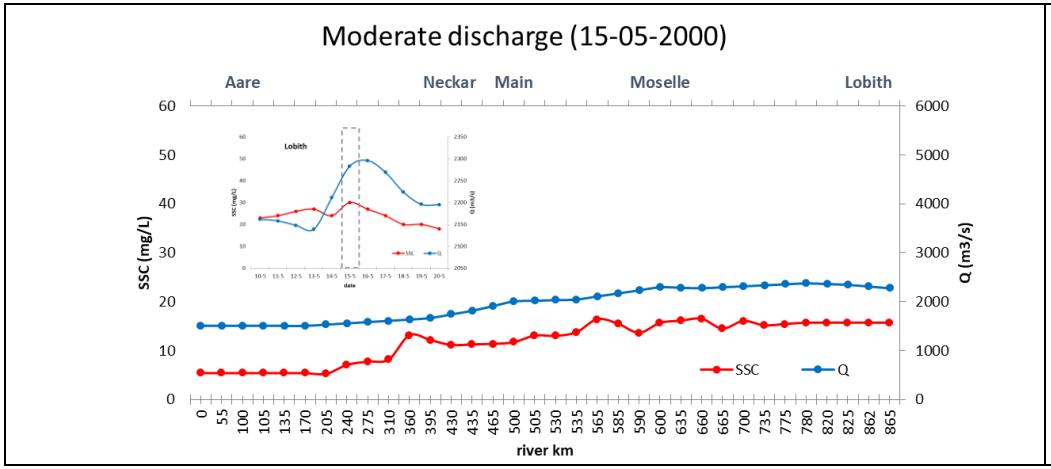

Description:

SSC increased in the downstream direction, especially at tributary confluence locations.

- There is a substantial increase 2 folds of SSC (10 mg/L) at impoundment section
- Neckar found less contribute to increasing of SSC, which only 1 mg/L
- At Middle Rhine, the Main River delivers substantially approximately 2 mg/L
- The transport of SSC from Moselle even increased strongly to about 5 mg/L
- Further downstream, the changes of SSC are much stable and disappeared completely after km 735, without sudden jumps at tributary confluences, where several small tributaries such as the Ruhr River, the Lippe River, and The Sieg River lie at the Rhine River

Neckar-km 430 (Figure.-b)

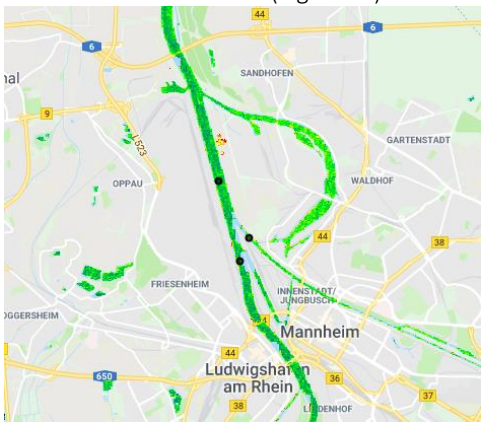

Main- km 500 (Figure.-c)

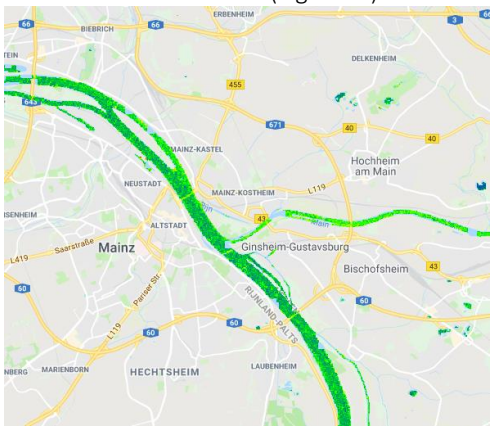

Koblenz Mosel-km 600 (Figure.-d)

Legend

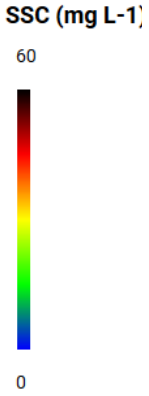

Moderate discharge (10-05-2001)

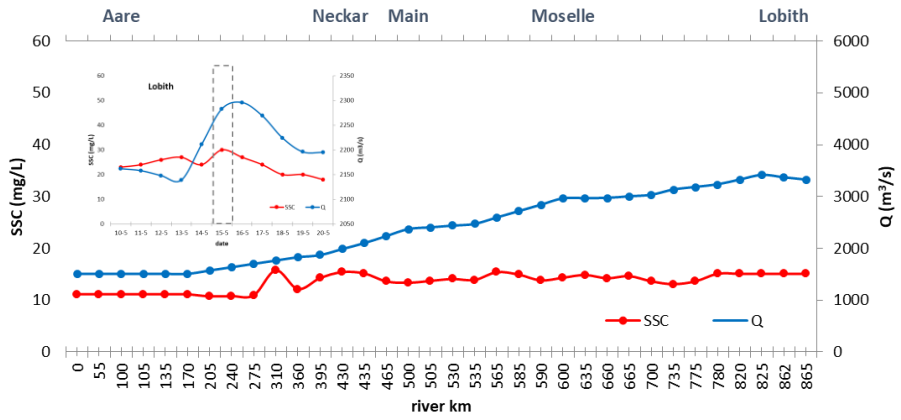

Description:

SSC increased in the downstream direction, especially at tributary confluence locations.

- There is a substantial increase of 5 mg/L at impoundment section
- Neckar contributes to increasing of SSC, which is 1 mg/L
- At Middle Rhine, the Main River delivers substantially approximately 2 mg/L
- The transport of SSC from Moselle even increased strongly to about 2 mg/L
- Further downstream, the changes of SSC are much stable and disappeared completely after km 735, without sudden jumps at tributary confluences, where several small tributaries such as the Ruhr River, the Lippe River, and The Sieg River lie at the Rhine River

Neckar-km 430 (Figure.-b)

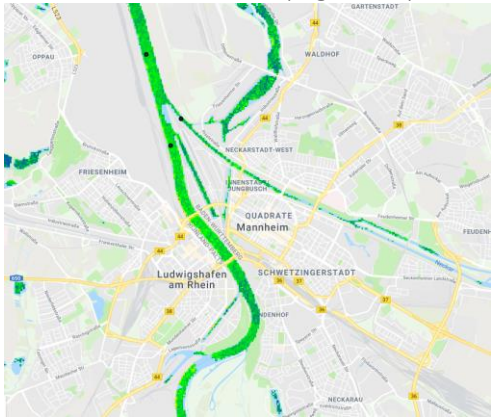

Main-km 500 (Figure.-c)

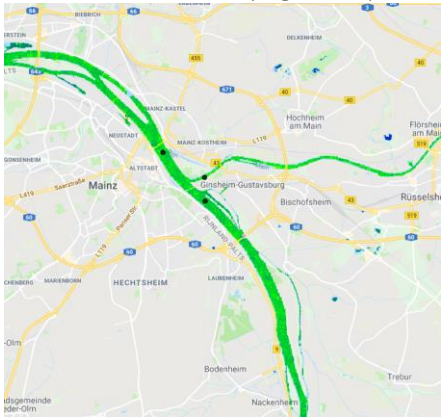

Koblenz Mosel-km 600 (Figure.-d)

Legend

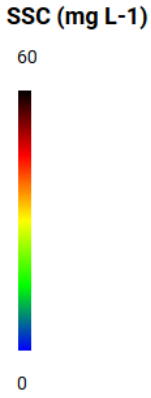

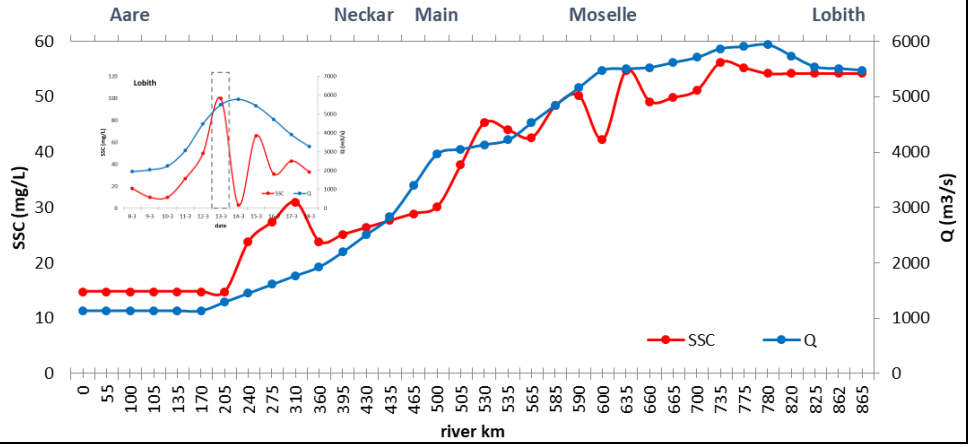

Description:

SSC increased in the downstream direction, especially at tributary confluence locations.

- There is a substantial increase of 20 mg/L at impoundment section
- Neckar contributes to increasing of SSC, which is 5 mg/L
- At Middle Rhine, the Main River delivers substantially approximately 20 mg/L
- The transport of SSC from Moselle even increased strongly to about 20 mg/L
- Further downstream, the changes of SSC are much stable and disappeared completely after km 735, without sudden jumps at tributary confluences, where several small tributaries such as the Ruhr River, the Lippe River, and The Sieg River lie at the Rhine River

Neckar -km 430 (Figure.-b)

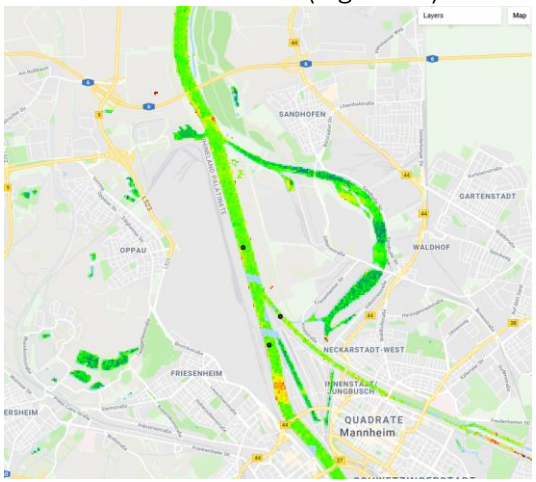

Main-km 500 (Figure.-c)

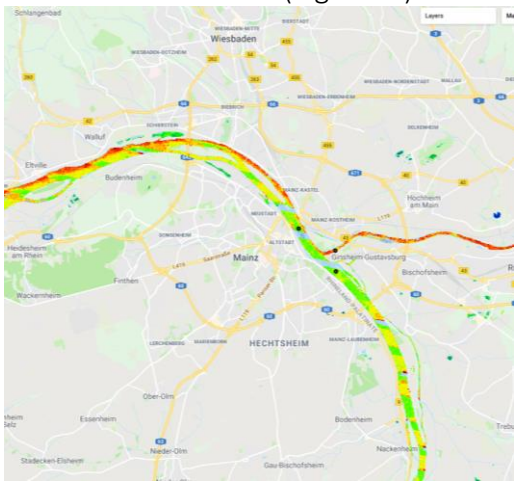

Koblenz Mosel-km 600 (Figure.-d)

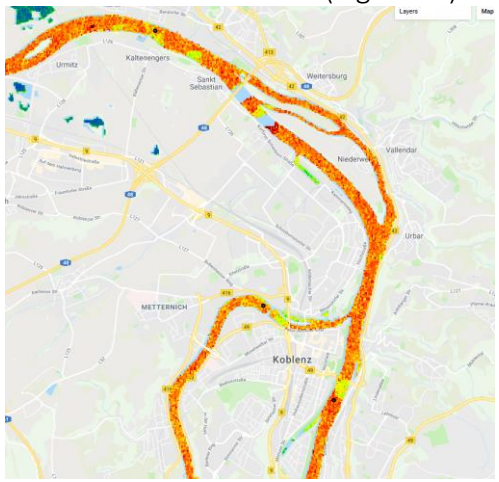

Legend

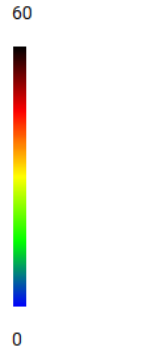

Moderate discharge (21-09-2006)

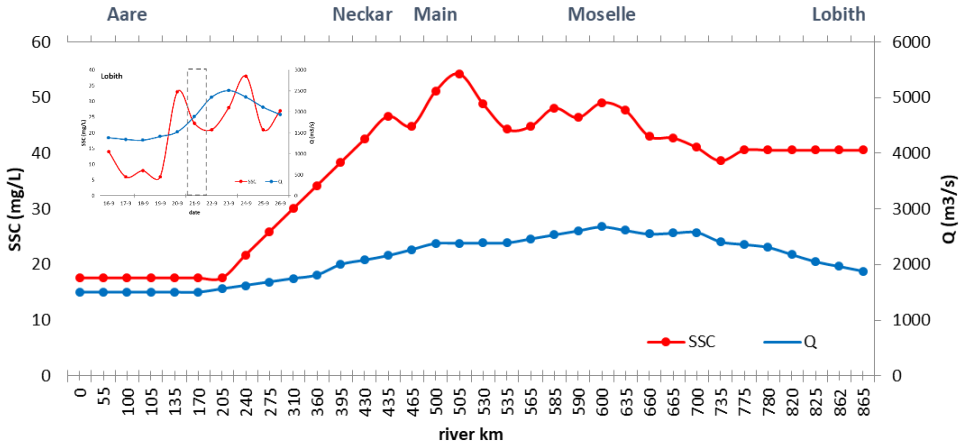

Description:

SSC increased in the downstream direction, especially at tributary confluence locations.

- There is a substantial increase of 20 mg/L at impoundment section
- Neckar contributes to increasing of SSC, which is 5 mg/L
- At Middle Rhine, the Main River delivers substantially approximately 5-10 mg/L
- The transport of SSC from Moselle even increased strongly to about 5 mg/L
- Further downstream, the changes of SSC are much stable and disappeared completely after km 735, without sudden jumps at tributary confluences, where several small tributaries such as the Ruhr River, the Lippe River, and The Sieg River lie at the Rhine River

Neckar-km 430 (Figure.-b)

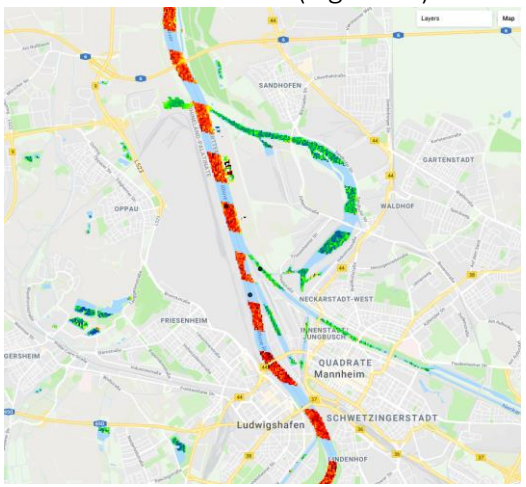

Main-km 500 (Figure.-c)

Koblenz Mosel-km 600 (Figure.-d)

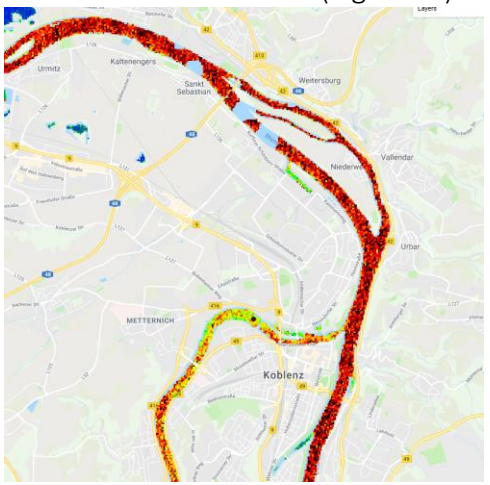

Legend

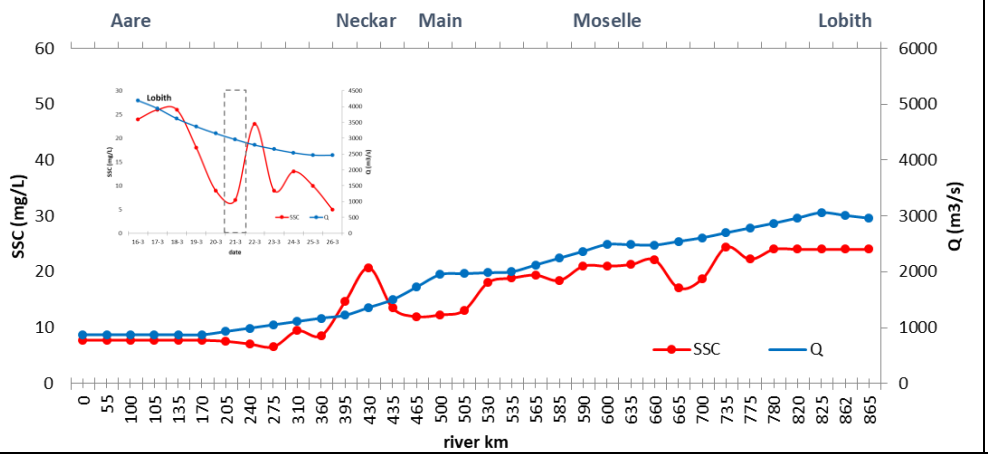

Description:

SSC increased in the downstream direction, especially at tributary confluence locations.

- There is a substantial increase of 5 mg/L at impoundment section
- Neckar contributes to increasing of SSC, which is 5 mg/L
- At Middle Rhine, the Main River delivers substantially approximately 5 mg/L
- The transport of SSC from Moselle even increased strongly to about 3 mg/L
- Further downstream, the changes of SSC are much stable and disappeared completely after km 735, without sudden jumps at tributary confluences, where several small tributaries such as the Ruhr River, the Lippe River, and The Sieg River lie at the Rhine River

Neckar-km 430 (Figure 5-b)

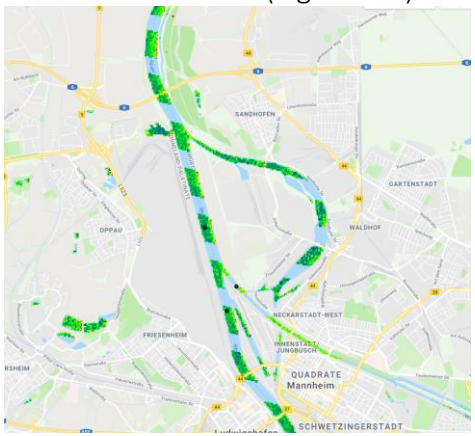

Main-km 500 (Figure 5-c)

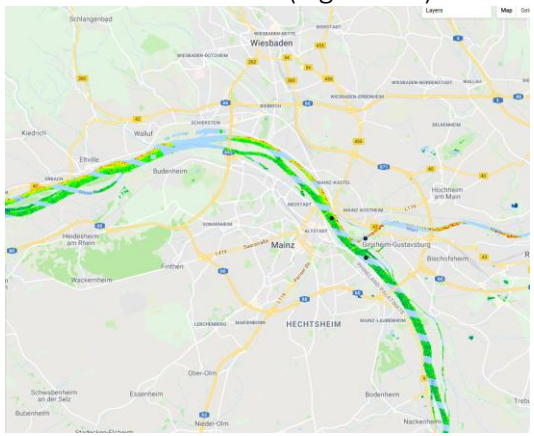

Koblenz Mosel-km 600 (Figure 5-d)

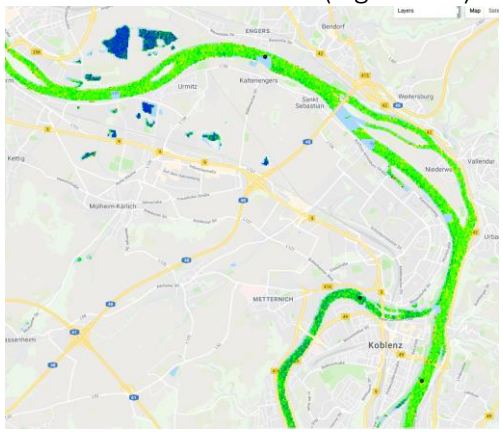

Legend

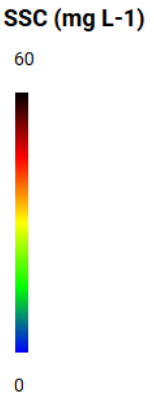

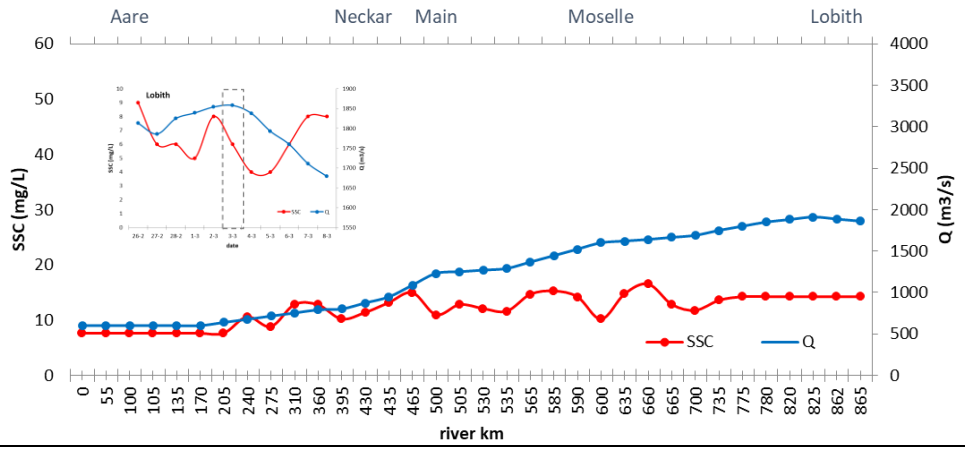

Description:

SSC increased in the downstream direction, especially at tributary confluence locations.

- There is a substantial increase of 5mg/L at impoundment section
- Neckar contributes to increasing of SSC, which is 3 mg/L
- At Middle Rhine, the Main River delivers substantially approximately 3 mg/L
- The transport of SSC from Moselle even increased strongly to about 5 mg/L
- Further downstream, the changes of SSC are much stable and disappeared completely after km 735, without sudden jumps at tributary confluences, where several small tributaries such as the Ruhr River, the Lippe River, and The Sieg River lie at the Rhine River

Neckar -km 430 (Figure.-b)

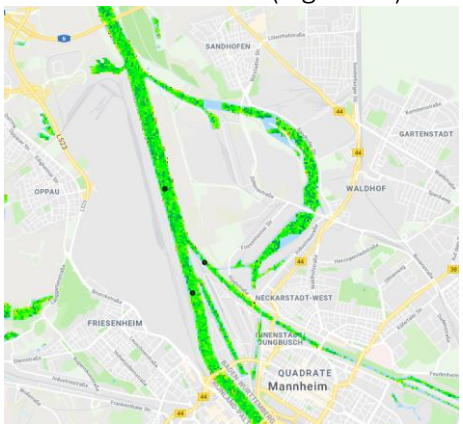

Main-km 500 (Figure.-c)

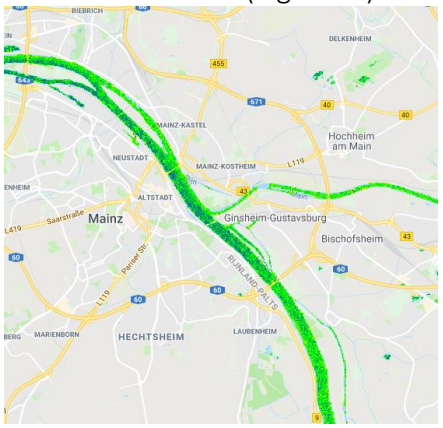

Koblenz Mosel-km 600 (Figure.-d)

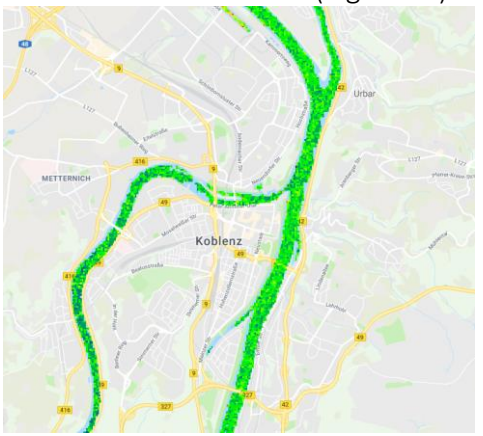

Legend

2. Suspended-sediment sources under low water

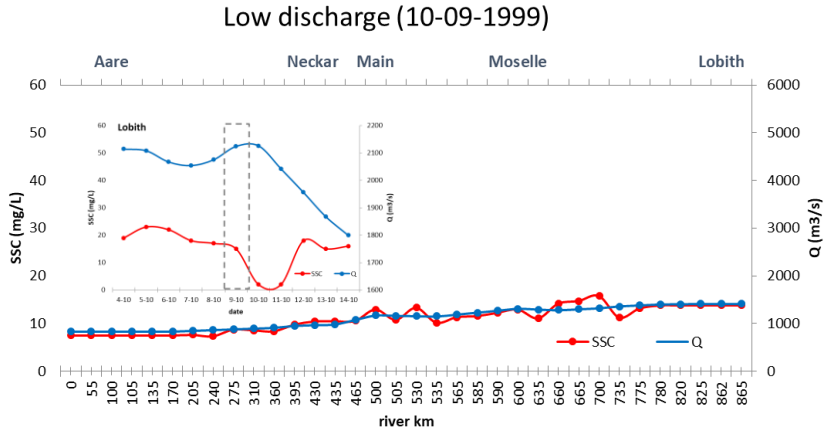

Description:

SSC increased in the downstream direction, especially at tributary confluence locations.

- There is a slight increase of 2 mg/L at impoundment section
- Neckar contributes to increasing of SSC, which is 1 mg/L
- At Middle Rhine, the Main River delivers substantially approximately 5 mg/L
- The transport of SSC from Moselle even increased strongly to about 3 mg/L
- Further downstream, the changes of SSC are much stable and disappeared completely after km 735, without sudden jumps at tributary confluences, where several small tributaries such as the Ruhr River, the Lippe River, and The Sieg River lie at the Rhine River

Neckar-km 430(Figure.-a)

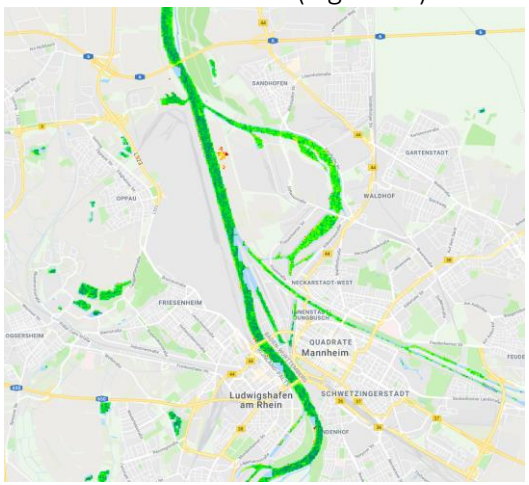

Main-km 500 (Figure.-c)

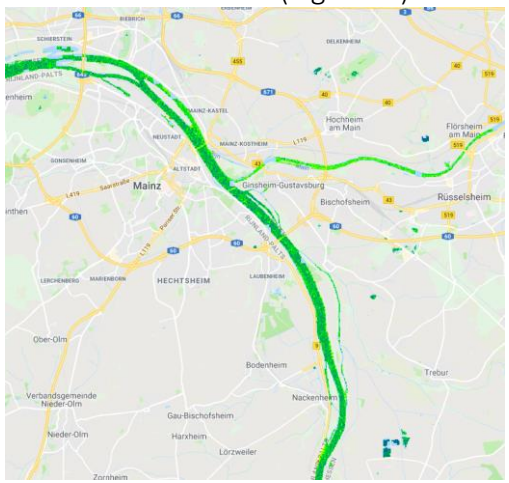

Koblenz Mosel -km 600 (Figure.-d)

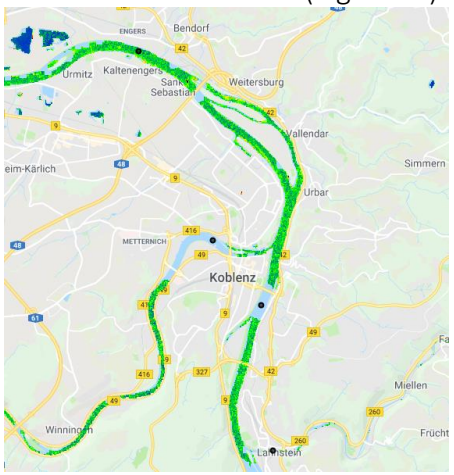

Legend

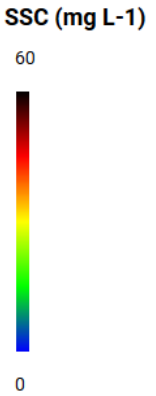

Low discharge (19-07-2003)

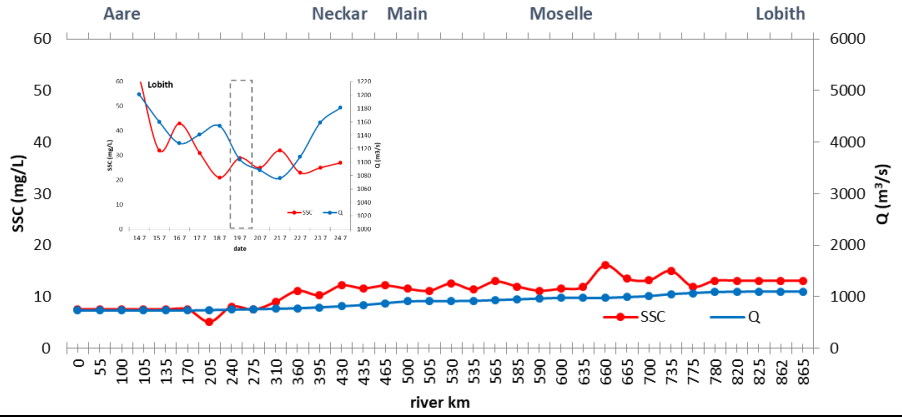

Description:

SSC increased in the downstream direction, especially at tributary confluence locations.

- There is a substantial increase of 8 mg/L at impoundment section
- Neckar contributes to increasing of SSC, which is 3 mg/L
- At Middle Rhine, the Main River delivers substantially approximately 5 mg/L
- The transport of SSC from Moselle even increased strongly to about 3 mg/L
- Further downstream, the changes of SSC are much stable and disappeared completely after km 735, without sudden jumps at tributary confluences, where several small tributaries such as the Ruhr River, the Lippe River, and The Sieg River lie at the Rhine River

Neckar -km 430 (Figure.-a)

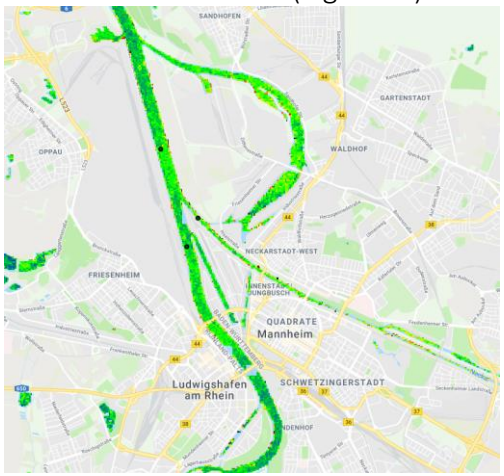

Main-km 500 (Figure.-c)

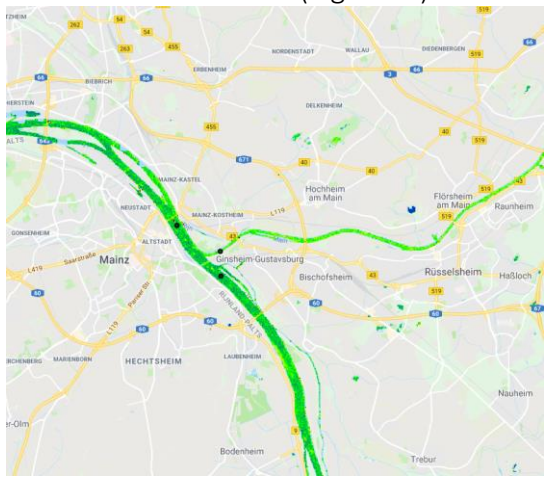

Koblenz Mosel -km 600 (Figure.-d)

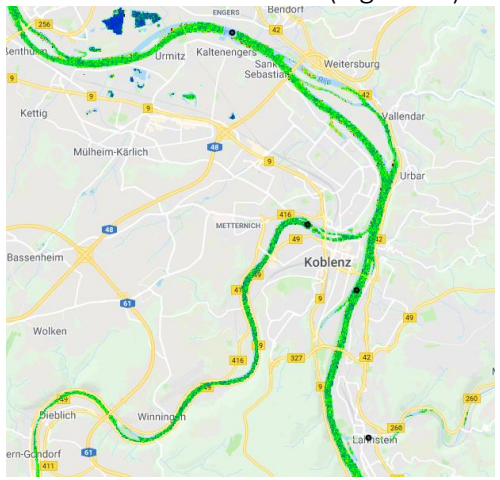

Legend

Low discharge (05-05-2008)

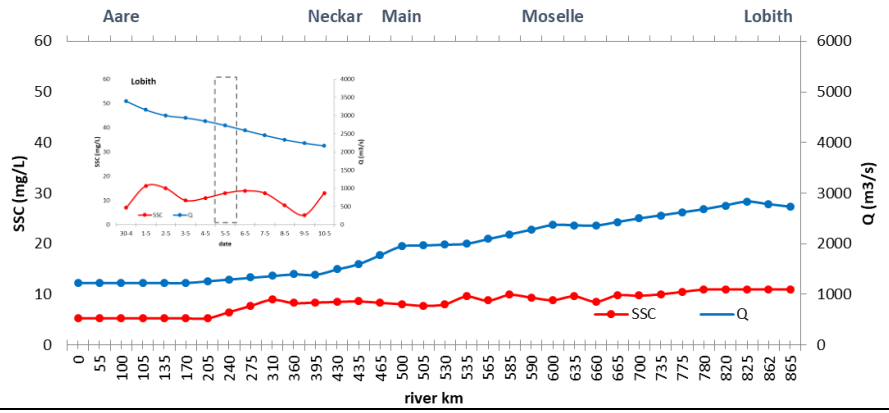

Description:

SSC increased in the downstream direction, especially at tributary confluence locations.

- There is a substantial increase of 10 mg/L at impoundment section
- Neckar contributes to increasing of SSC, which is 2 mg/L
- At Middle Rhine, the Main River delivers substantially approximately 3 mg/L
- The transport of SSC from Moselle even increased strongly to about 2 mg/L
- Further downstream, the changes of SSC are much stable and disappeared completely after km 735, without sudden jumps at tributary confluences, where several small tributaries such as the Ruhr River, the Lippe River, and The Sieg River lie at the Rhine River

Neckar-km 430(Figure.-a)

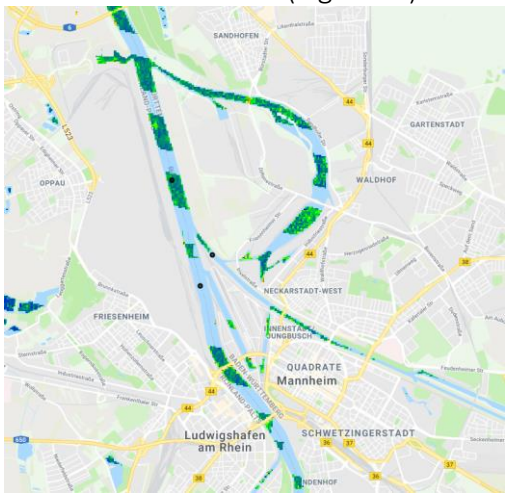

Main -km 500 (Figure.-c)

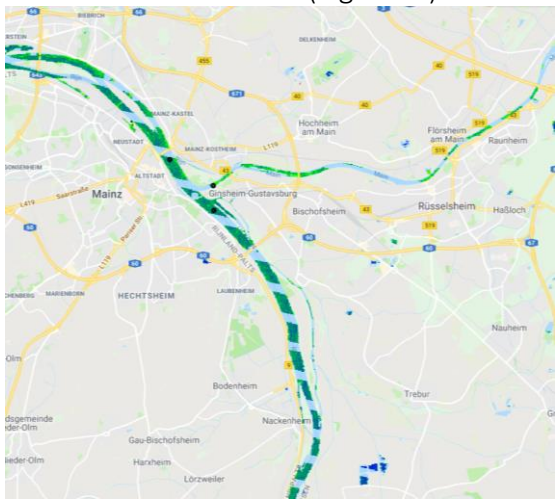

Koblenz Mosel -km 600 (Figure.-d)

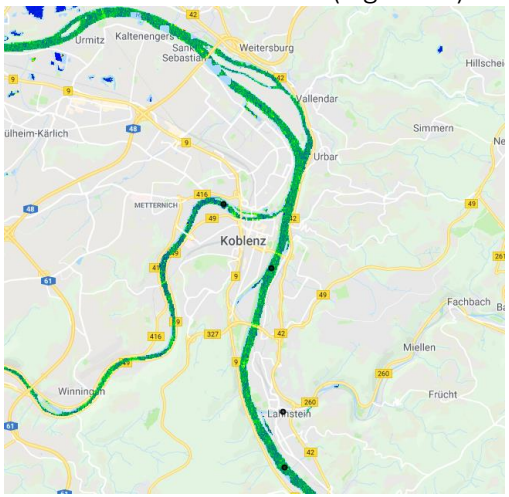

Legend

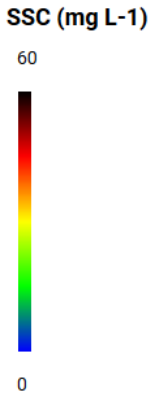

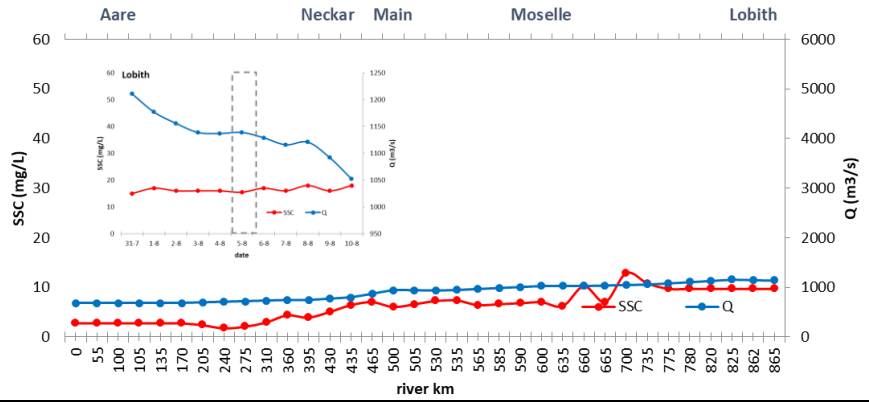

Description:

SSC increased in the downstream direction, especially at tributary confluence locations.

- There is a substantial increase of 5 mg/L at impoundment section
- Neckar contributes to increasing of SSC, which is 2 mg/L
- At Middle Rhine, the Main River delivers substantially approximately 3 mg/L
- The transport of SSC from Moselle even increased strongly to about 2 mg/L
- Further downstream, the changes of SSC are much stable and disappeared completely after km 735, without sudden jumps at tributary confluences, where several small tributaries such as the Ruhr River, the Lippe River, and The Sieg River lie at the Rhine River.

Neckar-km 430 (Figure -b)

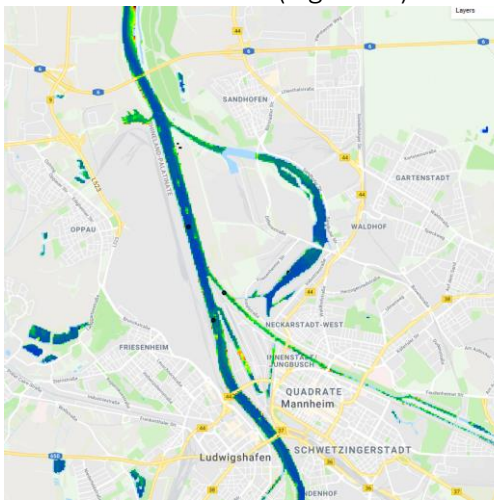

Main -km 500 (Figure -c)

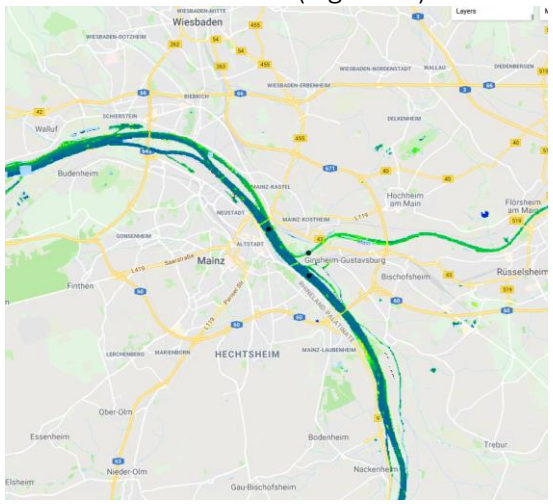

Koblenz Mosel -km 600 (Figure -d)

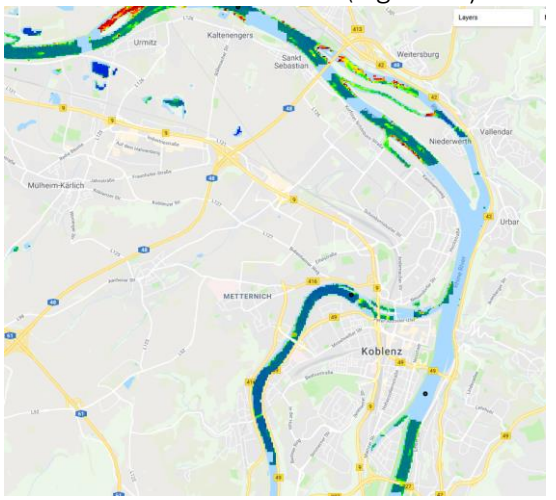

Legend

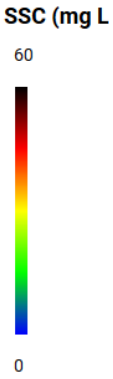

Neckar-km 430 (Figure -b)

Main -km 500 (Figure -c)

Koblenz Mosel-km 600 (Figure -d)